Fretting behaviour of Ti6Al4V/ Ti6Al4V contact for applications to modular junctions in hip implants

Submitted in Partial Fulfilment of the Requirements for the Degree of Master in Mechanical Engineering in the speciality of Production and Project

Author

Joana Filipa Jesus Pereira

Advisors

Amílcar Ramalho

Vincent Fridrici

Philippe Kapsa

Jury

President	**Professor Doutor José António Martins Ferreira** **Professor Catedrático da Universidade de Coimbra**
Vowel	**Professor Doutor Albano Augusto Cavaleiro Rodrigues de Carvalho** **Professor Catedrático da Universidade de Coimbra**
Advisor	**Professor Doutor Amílcar Lopes Ramalho** **Professor Associado c/ agregação da Universidade de Coimbra**

Laboratoire de Tribologie et Dynamique des Systèmes – École Centrale de Lyon

Coimbra, Setembro 2015

"The only way to do great work is to love what you do."

Steve Jobs

ACKNOWLEDGEMENTS

The following research work was only made possible due to the collaboration and support of several people to whom I cannot but express my recognition.

First and foremost, I would like to express my deepest gratitude to my excellent advisor, Professor Vincent Fridrici, for his guidance, support and endless patience during my internship in École Centrale de Lyon.

I am also grateful to my co-supervisor, Professor Phillipe Kapsa, for his insightful comments on my thesis and research.

To Professor Amílcar Ramalho for the opportunity that was given me to develop my research work at the LTDS – École Centrale de Lyon. For the valuable knowledge he passed on, his scientific rigour and for constant support.

To the whole LTDS community who proved themselves receptive and helpful.

To Cátia, Rafael and Beto for all their support during my stay in Lyon, the great coffee breaks and laughs, for maintaining that special work atmosphere and for making my life happier.

I would also like to thank Ricardo, my source of strength, for helping me in the most difficult moments during my academic path and for believing in me unconditionally.

To my parents, for their unshakable confidence in my future and for their many sacrifices which enabled me to have this opportunity. To my brothers for their comforting words and to my sister for all her support and understanding.

Finally, I would like to thank all my good friends for their encouragement and understanding throughout the years.

Abstract

This study arises as an answer to the need to minimize the collateral effects of the application of modular prosthesis of the hip implant and to try to create solutions that allow maintaining their reliability with the passing of time.

The present dissertation has as its objective the study of friction and wear on contact between the neck adapter and the stem of the modular prosthesis, subject to the phenomenon of fretting. Beyond that, it also has the objective of investigating the influence of the displacement amplitude, the contact pressure, number of cycles and roughness of the surfaces on the behaviour of the friction coefficient, dissipated energy and wear volume. The choice of the type of test to run, as well as the conditions of the test and the materials used have as their basis previously performed studies, which supply decisive information for the adequate selection of the test parameters.

Thus, fretting tests were performed with a cylinder on flat contact. On this contact interface, the cylinder, which remains static, represents the stem, and the plane, in relative motion, represents the neck adapter of the prosthesis. This contact can be performed with a flat that has roughness similar to that of the cylinder, which is perpendicular to the direction of movement, or with a flat with transversal roughness.

On a first phase, an analysis was performed on the surfaces of the components being studied as to validate the conditions of the surface of the tested samples. In sequence, after the fretting tests, one proceeded with the analysis of the wear scars and the occurrence of possible cracks using optical microscopy and with surface measuring instruments.

Keywords: Modular hip prosthesis, Fretting, Wear, Cracks, Friction Coefficient, Roughness.

Resumo

Este estudo surge como resposta à necessidade de minimizar os efeitos colaterais aquando da aplicação das próteses modulares da anca e de tentar criar soluções que permitam manter a sua fiabilidade com o passar do tempo.

A presente dissertação tem como objetivo o estudo do atrito e do desgaste no contacto entre o colo e a haste da prótese modular, sujeitos ao fenómeno de fretting. Além disso, tem também o objetivo de averiguar a influência da amplitude de deslocamento, pressão de contacto, número de ciclos e rugosidade das superfícies no comportamento do coeficiente de atrito, da energia dissipada e do volume de desgaste. A escolha do tipo de ensaio a realizar, bem como das condições de ensaio e materiais tem por base estudos anteriormente realizados, que fornecem informações decisivas para a seleção adequada dos parâmetros de teste.

Assim, foram realizados testes de fretting com contacto cilindro-plano. Nesta interface de contacto, o cilindro, que permanece estático, representa a haste e o plano, em movimento relativo, representa o colo da prótese. Este contacto pode ser realizado com um plano com rugosidade semelhante à do cilindro, ou seja, perpendicular à direção de movimento, ou com um plano com rugosidade transversal.

Numa primeira fase, realizou-se uma análise às superfícies dos componentes em estudo de forma a validar as condições de superfície das amostras testadas. Seguidamente, após os testes de fretting, procedeu-se à análise das marcas de desgaste e da ocorrência de possíveis fissuras recorrendo a microscopia ótica e instrumentos de medição da superfície.

Palavras-chave: Prótese modular da anca, Fretting, Desgaste, Fissuras, Coeficiente de atrito, Rugosidade.

Résumé

Cette étude s'agit une réponse à la nécessité de minimiser les effets de bord tant de l'application des prothèses modulaires de la hanche et d'essayer de développer des solutions qui permettent de maintenir sa fiabilité au fil du temps.

Cette thèse a comme objective l'étude de la friction e de l'usure dans le contact entre le col e l'haste de la prothèse modulaire, sous le phénomène de freeting. Dans un outre côte, cette thèse a aussi l'objective de comprendre l'influence de l'amplitude du déplacement, pression de contact, le nombre de cycles e rugosité des surfaces dans le comportement de la friction, de l'énergie dissipé et du volume de l'usure. Le choix du type d'expérience à réaliser, aussi bien que des conditions d'essaye et les matériaux est basée dans les études précédents, qui ont fourni des informations décisives pour la bonne sélection des paramètres de teste.

Ainsi, ils ont été réalisés des tests de freeting avec contact cylindre-plan. Dans cette interface de contact, le cylindre, qui se reste statique, il représente l'haste et le plane, en mouvement relatif, représente le col de la prothèse. Ce contact peut être réalisé avec un plan contenant une rugosité pareille à celle du cylindre, c'est-à-dire, perpendiculaire à la direction du mouvement, ou avec un plan contenant une rugosité transversale.

Dans une première étape, il s'été réalisé une analyse aux surfaces des components en étude pour valider les conditions de surface des échantillons qui ont été testé. Ensuite, après les tests de freeting, il s'été procédé à l'analyse des marques d'usure e de l'occurrence des éventuels fissures en utilisant la microscopie optique e des instruments de mesure de la surface.

Mont clés: Prothèse modulaire de la hanche, Freeting, Usure, Fissures, Coefficient de friction, Rugosité.

Contents

LIST OF FIGURES

LIST OF TABLES

SIMBOLOGY AND ACRONYMS

Simbology

E_d – Dissipated energy, J

N_c – Number of fretting cycles

S_a – 3D initial surface average roughness, nm

S_{ku} – 3D Kurtusis factor for roughness

S_{sk} – 3D Skewness factor for roughness

V_w – Wear volume, mm^3

p_0 – Maximum Hertzian's contact pressure, MPa

δ^* – Displacement amplitude, µm

δ_0 – Sliding amplitude, µm

δ_t – Displacement amplitude of transition, µm

E – Young's modulus, GPa

L – Width of the contact, mm

P – Normal force, N

Q – Tangential force, N

R – Cylinder radius, mm

a – Hertzian's contact radius, mm

f – Frequency, Hz

δ – Displacement, µm

μ – Friction coefficient

ν – Poisson ratio

Acronyms

ASTM – American Society for Testing and Materials

CETIM – Technical Center for the Mechanical Industry

DEM – Departamento de Engenharia Mecânica

FCTUC – Faculdade de Ciências e Tecnologia da Universidade de Coimbra

GS – Gross slip regime

LTDS – Laboratoire de Tribologie et Dynamique des Systèmes

LVDT – Linear Variable Differential Transformer

NR – Normal roughness

PS – Partial slip regime

TR – Transversal roughness

1. INTRODUCTION

Total hip arthroplasty (Figure 1.1) is intended to replace the hip joint that joins the femur to the hipbone with a positive impact on the patient's quality of life. This joint is considered the most powerful in the human body due to the forces to which it is subjected.

Figure 1.1. Total hip arthroplasty [1].

The hip joint allows producing a wide range of movements such as flexion and extension around the transversal axis, abduction and adduction that is the movement around the anterior posterior axis and lateral rotation and medial rotation around the vertical axis [2] (Figure 1.2).
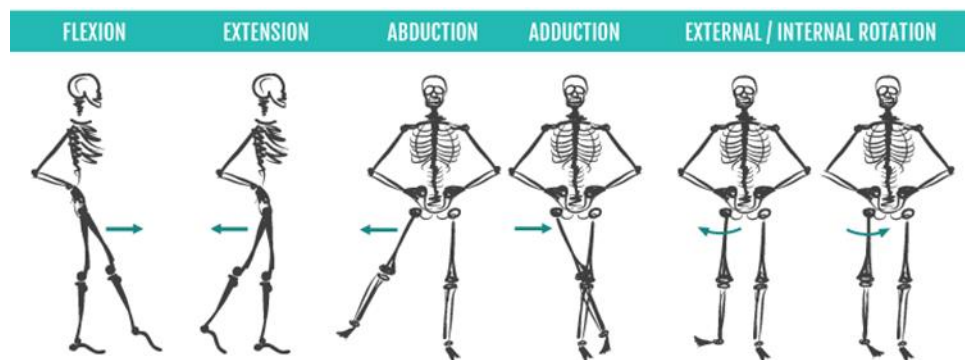
Figure 1.2. Possible hip movements illustration [3].

The combined effects of these movements, fretting corrosion, patient size, patient weight and activity level may have all played integral roles in creating an environment susceptible to the initiation and perpetuation of fatigue failure of the material. In order to avoid revision surgeries and morbidity cause by the failure of the prosthesis, a careful preoperative planning should be done.

Even if the hip implants are supposed to give the patients a good quality of life, there are some side effects related to that, such as:

- Metallosis (metal poisoning)
- Corrosion
- Tissue damage, or death
- Bone loss
- Pseudotumor formation
- Severe pain in the hip joint
- Inflammation
- Swelling
- Misalignment or dislocation of the hip joint
- Need for revision surgery

Taking into account all these possible inconveniences, it is necessary to review this technology in order to minimize inherent collateral damage in their application and try to create solutions that allows maintaining the same reliability as new prosthesis over the time [4].

1.1. Modular junction

Since 1970's modular head neck components have been used to vary head length and diameter independently of the stem. In the 1990's the first modular neck adapter was used for intraoperative adjustment of column-caput-diaphysis angle and femoral ante version to optimise offset and leg length, irrespective of the hip stem implanted. According to this new formulation the prosthesis is divided in three pieces, head, neck adapter and stem (Figure 1.3) that facilitates the replacement when in revision surgery. However, it is created another contact interface that is propitious to fretting behaviour, which is the main reason for its rejection from medical professionals [5].

Modular junctions in hip implants are designed with an interchangeable femoral neck that includes a metal-on-metal component and even it offers several distinct advantages, adding a new interface is related to the reduced of mechanical resistance, fretting, corrosion, accumulation of metal debris in the body and material fatigue fracture [6].
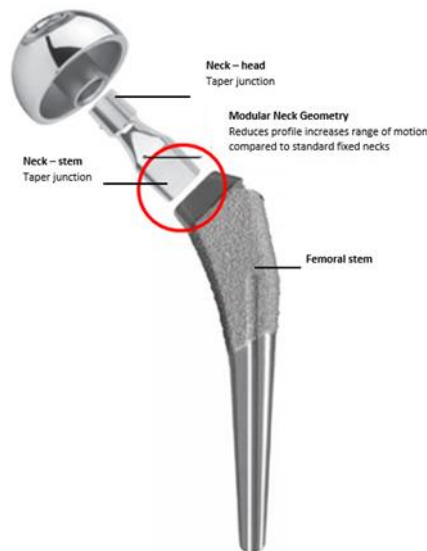
Figure 1.3. Modular hip prosthesis [7].

There are several failures recorded due to this design. For instance, it was recorded a failure [8] that occurred where the stem is in contact with the distal part of the modular neck (Figure 1.3). Another case report conducted [9] exposes another situation with a deformity at the neck-stem junction that suggested a femoral neck fatigue fracture.

An overview about the failure of the neck adapter and its possible reasons was conducted [10] and it was concluded that until the end of 2008 1.4% (n = 68) of the titanium alloy neck adapters failed after an average time in vivo of 24 months (Figure 1.4). All but one patients were male and most patients (59%) had a weight above 100 kg and an average body mass index (BMI) of 31.6 (24 to 42) (Figure 1.5).
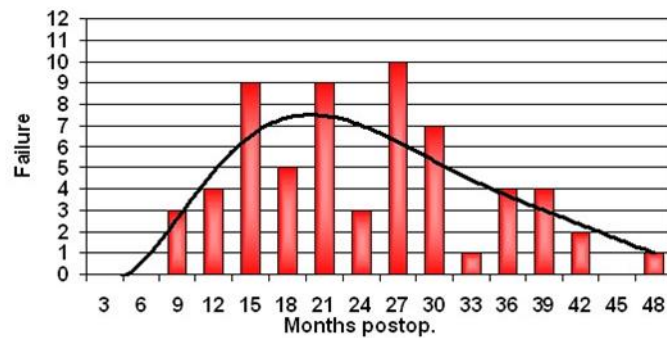
Figure 1.4. Occurrence of clinical neck failures in a postoperative time period in months [10].
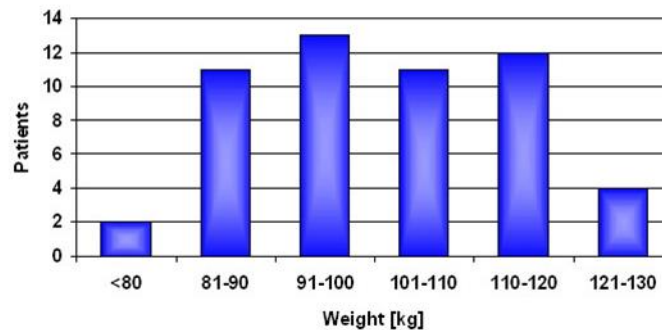
Figure 1.5. Correlation weight of patients and failures [10].

1.2. Materials

Despite the variability of hip implants on the market, for modular models the materials for the stem and for the neck adapter relies on stainless steel, titanium alloy and cobalt chromium.

The advantages of AISI 316L stainless steel in comparison with other alloys used, such as titanium, are the lowest price and ease of acquisition with quality assurance. The disadvantages are related to the corrosion and susceptibility to a lower mechanical performance when subjected to cyclic tensional forces. New surface treatment technologies have benefit significantly this material, improving their performances [11].

Although cobalt chromium is very resistant to corrosion, it has about 1/3 fracture toughness compared to titanium alloys and increased tendency to release particles to the body [11].

Titanium alloys have high mechanical strength, better corrosion resistance than stainless steel, very good level of tolerance and a very close elasticity modulus to the one of

cortical bone. They are also more biocompatible. Titanium prostheses are manufactured by casting with forging about 1100 ºC with the objective of obtaining a fine crystalline structure. The disadvantage is mainly the high cost [11].

These materials offer a reduced wear rate, with less probability of inflammation and bone loss. However, due to the relative motion between the different parts of the implant, the wear products (submicroscopic particles, soluble metal ions) even reduced, are distributed throughout the body. This has raised concerns about long-term bio-compatibility.

The motion between two surfaces reduces the fatigue strength of the titanium significantly. This effect can be avoided by using cobalt-chromium [12]. In Figure 1.6 it is shown two neck adapters, the first one made of Co-Cr and the second one made of Ti6Al4V. For 10.000 cycles with a load between 230 and 4300 N, and a frequency of 1 Hz, it is possible to see that there are no surface damages in the cobalt-chromium neck adapter but there are some scratches in the titanium alloy component [13]. Besides that, for another study with similar parameters, for a contact load of 5300 N and a frequency of 1 Hz/ 15 Hz the neck adapter made of cobalt-based alloy did not break but the titanium alloy adapter fractured after 2,45 million cycles [10].

Even if it seems to be less risk of failure with Co-Cr neck adapters, when using it, there are some ions released that leads to genotoxic changes and it can also cause pseudotumors related to immune-allergic reactions.

Figure 1.6. H-Max neck adapters after mechanical testing. In the laterodistal area of Ti neck adapters slight scratches could be observed (bottom). No surface damages at the Co-Cr neck adapters were seen (top) [13].

Due to the fact that there is no consensus in the orthopaedic community regarding the best material, the choice generally comes down to the surgeon's experience as well as the preference with the implantation methods [14].

1.3. Fretting in modular junctions

Most of the side effects reported with the implementation of modular prosthesis arise from the release of particles through the body, which can cause, among others, severe metal poisoning and inflammation. The released particles are commonly due to the phenomenon of fretting that occurs when two surfaces are in contact, under load and in the presence of repeated relative surface motion, typically in the range 5–100 μm [15]. The ASM Handbook on Fatigue and Fracture defines fretting as: "A special wear process that occurs at the contact area between two materials under load and subjected to minute relative motion by vibration or some other force". One of the most critical areas for triggering this behaviour is between the stem and the neck adapter. The methods used to mitigate fretting damage are, for instance, change in design (design optimisation, geometrical modifications of components, NR/ TR), use of lubricants and application of surface engineering (surface treatments, coatings). When using the surface modification methods, there are at least five different mechanisms to increase fretting resistance: to induce a residual compressive stress, to decrease the friction coefficient, to increase hardness, to change surface chemistry and to increase surface roughness [16].

The friction between two surfaces causes mechanical wear and transfer of material that occurs due to adhesion between the bodies in the asperities, this is often followed by corrosion of the asperities and of the exposed metallic surfaces. When subjected to this behaviour, the surface layer of the component is degraded and therefore the surface and subsurface stress distributions are modified, which increases the roughness, reduces the fatigue strength of the materials and consequently make it more vulnerable to the growing of microcraks and the failure of the components.

Depending mostly on the displacement amplitude and on the normal force, fretting can occur with two main relative contact conditions, partial and gross slip which will be explained further ahead. Mixed slip regime is characterized by the change in the contact conditions from gross slip to partial slip as the number of cycles increases. The mixed slip regime is therefore enclosed between the transition boundaries which correspond to the initial and to the stabilized values of the friction coefficient respectively [17]. Stick regime is identified under low displacement amplitude. In this regime, very limited surface damage was observed [18].

For given conditions, the displacement amplitude for which the regime changes from partial slip to gross slip is called displacement amplitude of transition (Figure 1.7).
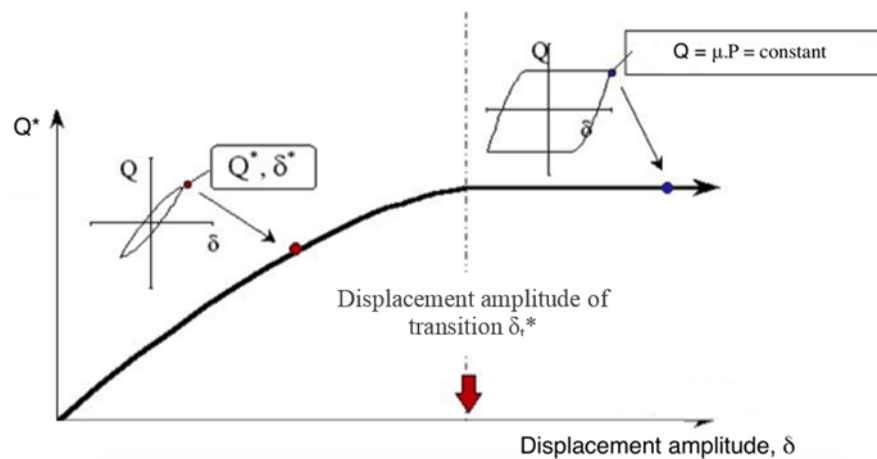
Figure 1.7. Transition between partial slip regime and gross slip regime [19].

When dealing with a cylinder on flat contact, the contact area between the two surfaces has a half width a, which is a function of the normal force, P, as established by the Hertzian contact model. Applying to the contact an alternative motion with a displacement amplitude, δ^* (Figure 1.8) there is going to be observed a fretting loop for each cycle, which relates the tangential force Q, that reflects the tangential stresses imposed at the contact, with a relative displacement δ (Figure 1.9). This loop allows knowing the regime of the test that is being performed, the dissipated energy, the coefficient of friction, among many other important parameters [19].
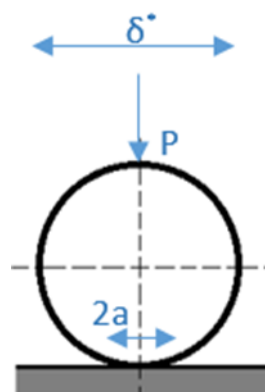
Figure 1.8. Representation of the ball on flat contact.
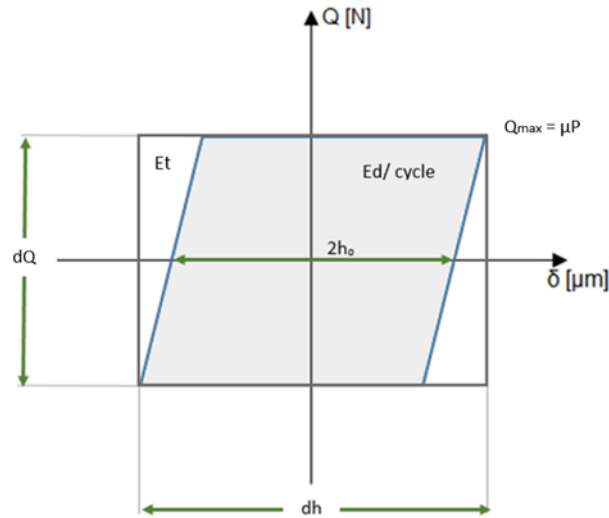
Figure 1.9. Theoretical representation of a fretting loop of a test with gross slip conditions and of variables that can be drawn from the loop.

The parameter h_0 is defined as the value of the displacement for a null tangential force. The dissipated energy, E_d , corresponds to the area contained within the cycle and it occurs through many mechanisms, for instance, creation of debris, temperature rise, cracking or plastic deformation. In the case of a perfectly rectangular cycle, the dissipated energy is defined as equation (1.1). And finally, the total energy E_t, corresponds to the area of the smallest rectangle containing the cycle [19].

$$E_d = 4.Q.\delta^*$$
(1.1)

It was verified that to obtain the output parameters, such as the dissipated energy, the software automatically corrected the effect of compliance taking into account the deflection of the system.

1.3.1.   Partial slip regime

If the displacement amplitude imposed to the contact is not enough to achieve the threshold friction force, the relative motion is limited to the external border of the contacting area, around a central adhesion part. This regime is characterized by an elliptical fretting cycle (Figure 1.10) where the displacement amplitude is lower than the displacement

amplitude of transition. The greater the displacement amplitude, the greater the magnitude of the tangential force and lower is the adhesion area [19]. In PS situation, the central zone of the contact, remains in stick condition, without the relative displacement and the external zone of contact is subjected to sliding (Figure 1.11) [20] The tangential force applied to the contact induces a shear distribution, q, which is superimposed on the distribution of contact pressure, p. In the areas of sliding and considering a Coulomb friction coefficient μ, it is verified the equation (1.2). In the stick zones, it is verified equation (1.3): the local relative displacement is supported by the deformation of the contact bodies. Thus in partial slip regime, the relation between the maximum tangential force Q^* and the normal force P, does not correspond to a coefficient of friction [19].

$$q = \mu . p \tag{1.2}$$

$$q < \mu . p \tag{1.3}$$

It is verified that for partial slip conditions there is not a significant amount of wear compared to gross slip conditions, and its location is mostly in the edges to the boundaries between the stick and slip zones. The risk of crack nucleation is therefore greater at the contact edges for small numbers of cycles and at the stick–slip boundaries for large numbers of cycles. In addition, the dramatic increase in the shear stress at the stick–slip boundaries increases the risk of nucleation of shear type cracks [15].
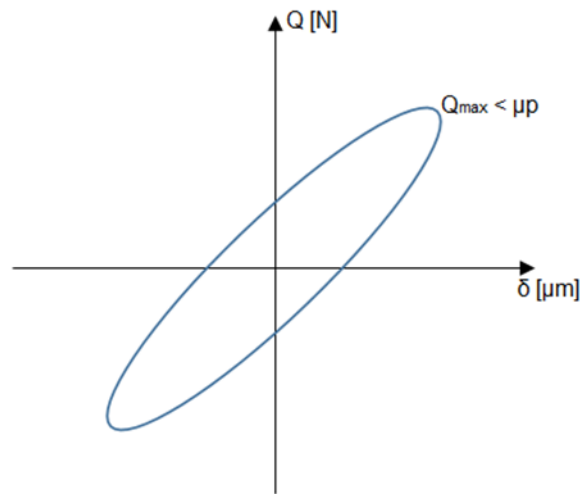
Figure 1.10. Schematic of variation of tangential force with displacement amplitude under in partial slip regime.
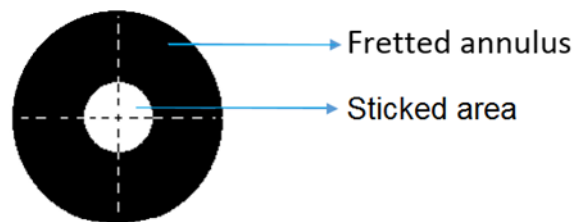
Figure 1.11. Top view of the ball on flat contact for tests in partial slip regime.

1.3.2. Gross slip regime

For this condition, fretting cycle is a parallelogram (Figure 1.12) where the displacement amplitude is higher than the displacement amplitude of transition. When the displacement amplitude is greater, there is no stick area and whole the contact area is in sliding (Figure 1.13). The maximum tangential force Q^* is independent of the displacement amplitude and the friction coefficient µ can then be defined as the ratio between the maximum tangential force Q^* and the normal force P [19].

For gross slip regime, the relative motion between surfaces induced severe modification of the contact geometry, in other words, the high wear rate leads to the contact edges, moving rapidly outwards leaving the material, previously at the contact edges, in a permanently compressive state, which prohibits fretting-fatigue crack initiation. This

suggests an explanation for wear being the predominant feature in gross slip with growth of a fretting fatigue crack being much less likely [15].
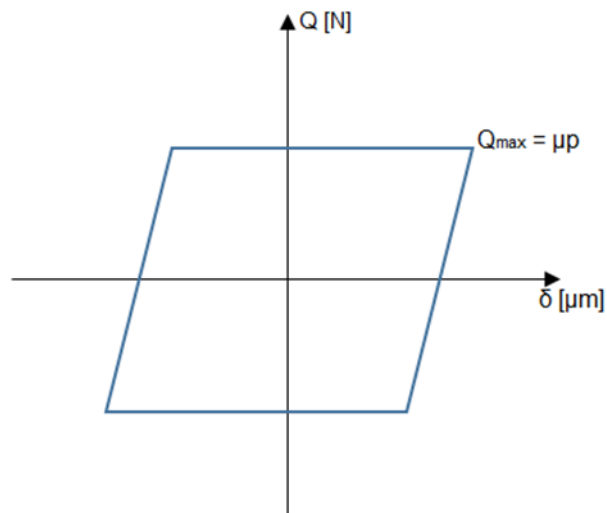
Figure 1.12. Schematic of variation of tangential force with displacement amplitude under in gross slip regime.
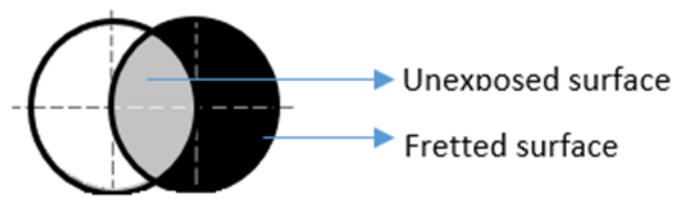
Figure 1.13. Top view of the ball on flat contact for tests in gross slip regime.

1.3.3. Influential parameters on the process

In order to analyse the behaviour of the materials during the process of fretting and to guarantee a correct choice of values to perform the tests, there should be a good background about the influential parameters on the process defined by the analysis of fretting cycles.

The input parameters are the displacement amplitude, the contact pressure, the number of cycles and the frequency that are chosen considering the type of contact that is

intended. One of the objectives of this work is to analyse the effect of the input parameters on the behaviour of the coefficient of friction, the dissipated energy and the wear volume.

1.3.3.1. Displacement amplitude

Displacement amplitude, δ^*, measured in microns, is a controlled parameter in the fretting tests. There are several possible measurement methods such as LVDT, laser or optical techniques. It is a measurement of distance of the motion of the moving specimen from its equilibrium position to the maximum value of its movement.

For a homogeneous contact of Ti6Al4V cylinder on flat configuration, after 10.000 cycles and a frequency of 10 Hz, the maximum crack propagation occurs for a displacement amplitude of ±22,5 μm and a contact pressure of 450 MPa [21].

Analysing the contact with a cylinder-on-flat configuration considering a frequency of 1 Hz, 6.000 cycles and a contact pressure of 398MPa changing the displacement amplitude from ±25 to ±50 μm [22] it is possible to conclude that it is shown clear indications of wear by particle detachment in the direction of fretting. It is expected that for higher displacement amplitude there will be more wear and less transfer of material [23] [24].

A previous study of finite elements made by CETIM [25], concluded that, for the neck adapter and according to ISO 7206-6, in contact conditions there will be a maximum displacement of ±100 μm.

1.3.3.2. Contact pressure

Since in this study the contact geometry involves a cylinder and a flat, the stress distribution is not uniform and there is need to use Hertz's theory in order to calculate the contact distribution.

Considering Hertz's theory, localized stresses that develop as curved surfaces come into contact and deform slightly under the imposed loads, causes deformation, which is dependent on the elastic properties of both materials in contact. Contact stresses are also a function of the normal contact force and the radius of the curvature of both bodies.

For a cylinder-on-flat contact the formulation for the contact pressure relies on the equations (1.4), (1.5) and (1.6).

$$\frac{1}{E^*} = \left[\frac{1 - \nu_1^2}{E_1}\right] + \left[\frac{1 - \nu_2^2}{E_2}\right] \qquad (1.4)$$

$$a = 2\left(\frac{PR}{\pi E^* L}\right)^{1/2}$$

(1.5)

$$p_0 = \frac{2P}{\pi L a} = \left(\frac{PE^*}{\pi RL}\right)^{1/2} \ (MPa)$$

(1.6)

Being E_1, E_2, ν_1 and ν_2 the Young's modulus and the Poisson ratio for the two components used, respectively. The normal force is represented by P, the maximum contact pressure by p_0, the radius of the cylinder is R, the width of the contact is L, and finally, the half width of the contact is represented by an a.

Previous studies made by CETIM [25] concluded that, for this study, the range of contact pressure should be from 300 to 800 MPa in order to make a good analysis of the surface.

Contact pressure has an important role on the wear rate, higher normal pressure will lead to higher local wear rate [26]. Another study [22] indicates that the contact pressure at the taper interface should be between 630 and 860 MPa to prevent wear and cracks for maximum expected micro motions between ±20 and ±50 μm. For 1 Hz and 6.000 cycles, the results of the fretting tests are shown in the Figure 1.14. To sum up, wear in gross slip was observed under high displacements and low contact pressure.

Figure 1.14. SEM micrographs showing the effect of normal force and displacement amplitude on the mode of fretting damage. "a"- There was observed wear; "b"- There were observed some cracks; "c" – There was no damage; "*"- There was no surface changes [22].

Assuming an overage body weight of 750 N, a loading cycle ranging between 300 N (346 Mpa) and 2300 N (958 MPa) simulates normal walking, while a cycle between 300 N (346 MPa) and 4200 N (1295 MPa) simulates the maximal conditions recorded during fast jogging [27]. As for walking upstairs, the hip contact force corresponds to 230 N (303 MPa) to 4300 N (1310 MPa) [13]. The range from 300 N to 3300 N (346 - 1148 MPa) is that proposed by ISO 7206/ 7:1993 standard for endurance tests on hip stems.

1.3.3.3. Number of cycles

A cycle goes from the equilibrium position to the maximum and minimum value, ending in the initial point. During a test it is executed as much cycles as it is required.

A previous study [27] relates the number of cycles and the applied load with the weight loss between a neck adapter and a stem, both made of Ti6Al4V. The tests were run in a bath of buffered Ringer solution at an approximately temperature of 37 ºC, with a frequency of 10 Hz, a load cycling ranging from 300 to 3300N for 5,5 and 20 million cycles. In Figure 1.16 is shown that the weight loss increases linearly with load. Note that it is

assuming that the experiment is in gross slip regime, otherwise with the increasing applied load the regime would change to partial slip and the wear would decrease. For Figure 1.15 the amount of weight loss is higher for the highest number of load cycles.
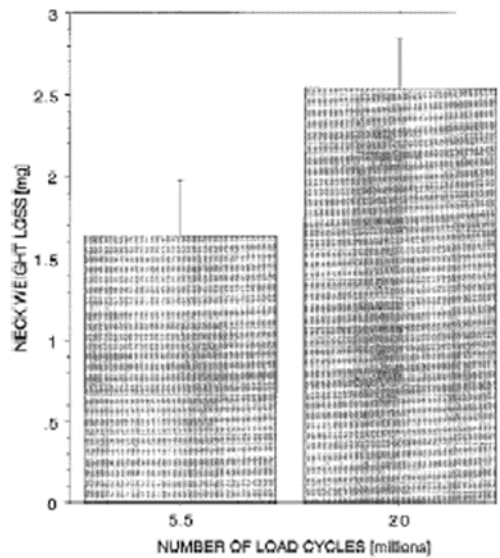
Figure 1.15. Effect of the number of load cycles: measured after 5,5 million cycles and 20 million cycles [27].
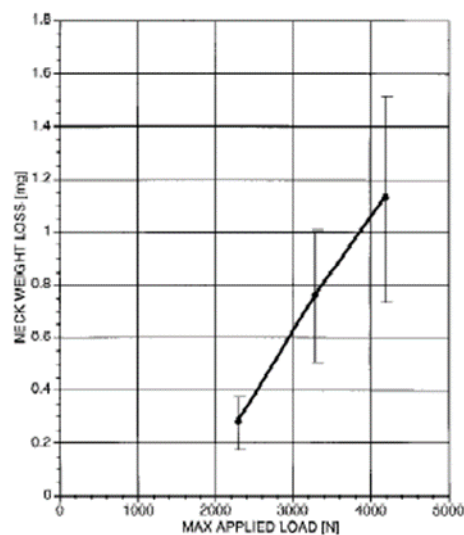
Figure 1.16. Effect of the load magnitude [27].

1.3.3.4.   Frequency

To reduce test duration, the frequency, measured in Hertz, is usually fixed to the highest value that does not interfere with the experiment [27]. A previous study showed that the frequency should be kept below 15 Hz to avoid the re-passivation of titanium alloy [10]. Besides that, another work showed that the damage produced in the head-stem modularity tested *in vitro* at a frequency of 10 Hz was similar to that retrieved from patients [28]. It was also studied the frequency dependence of fretting wear between 1 Hz and 8 Hz. The results showed that high wear rates can be obtained at low frequencies [29].

1.3.3.5.   Surface roughness

In many industrial applications, it is not possible to control the fretting degradation process. Therefore, the initial design of such elements is the only way to prevent or reduce fretting phenomenon and surface damage. If it is not possible to modify the contact loading to reduce fretting degradation, the initial roughness could be optimised [20].

Surface roughness can be defined by the deviation in normal direction from its ideal form. In case the deviations are big, the surface is rough; otherwise, the surface is smooth. Normally, there are three main parameters used to describe the roughness of a surface. The 3D surface roughness is the S_a and it is measured in nanometres. The Skewness factor, S_{sk}, is known for being the profile asymmetry factor that allows checking the wear resistance of the surface. Lastly, the Kurtosis factor, S_{ku}, goes over the profile flattening and as for the previous one is a dimensionless parameter. Further, additional explanation of these two roughness factors is presented in Annex A [30].

Initial surface roughness has a significant influence on friction and wear process [20]. By common sense, rough surfaces usually wear more quickly and have higher friction coefficients than smooth surfaces. Moreover, the roughness of the surface gives information about its susceptibility to crack nucleation, corrosion and adhesion.

Under fretting conditions, initial surface roughness can be a major factor in determining sliding conditions at the interface and the corresponding fretting damage mode, i.e., cracking or wear.

During wear process, degradation of the surface modifies the initial geometrical state of the interface, which affects the sliding conditions and can lead to change in sliding regime [26]. When the initial roughness is removed, wear process should continue at constant rate.

Even if one of the motivations in the manufacturing industry is decrease the roughness of the materials, it can be a difficult task due to the costs involved in the process. Decrease the roughness of a surface will usually increase its manufacturing costs [31].

Titanium alloy is a material that has a high tendency to adhesion. Thus, when associate wear volume with the dissipated energy, it is not achieved a straight line, which means that the dissipated energy is not the only parameter for wear. For fretting tests, in order to have wear at the end of test it is required to be generated wear debris (driven by the dissipated energy) and that these debris are removed from contact, otherwise, despite the existence of wear debris, there is obtained few wear volume. For materials with high adhesion properties, such as titanium alloy, it is more difficult to eliminate these debris as they can be transferred to the counter body and then stay in the contact.

A previous study [31] says that, if the displacement amplitude is high, for the same dissipated energy, it will be more wear volume. This is because, when there is high values of displacement amplitudes, it is easier for the debris to be ejected, generating more wear volume. According to this study, Table 1.1 summarizes the different ways for wear. Having this into consideration, the wear evolution can be normalized on a linear single curve as a function of the displacement amplitude multiplied by the total dissipated energy during the process.

Table 1.1. Summary of the different ways of wear, taking into account the dissipated energy and the displacement amplitude

E_d / δ	Low	High
High	Few debris are formed and they can eject easily: **Medium wear**	Many debris are formed and they can eject easily: **High wear**
Low	Few debris are formed and they cannot eject easily: **Low wear**	Many debris are formed and they cannot eject easily: **Medium wear**

This approach that will be confirmed later in this dissertation facilitates the evaluation of wear and enables to conclude that the wear kinetics can be described through a single wear law [31].

The following equation (1.7) describes this theory. The parameter V represents the wear volume, δ the sliding amplitude and E_d the total dissipated energy during the process.

$$V = f(\delta . \sum E_d) \qquad (1.7)$$

Note that this theory only makes sense for tests in gross slip regime, since in partial slip regime, dissipation of energy can go through crack initiation.

1.4. Friction and wear phenomena

The coefficient of friction is a dimensionless parameter that expresses the opposition that two surfaces have when sliding one over the other. For titanium alloy the normal value is quite high, between, 0,8 and 1,0 [23] [24].

During this study the coefficient of friction is going to be determined experimentally by the ratio between the tangential force and the normal force, for tests in gross slip regime, which is the regime with wear as the principal consequence.

For the experiments, with titanium alloy materials, it is expected an initial rise in friction mainly due to the strong adhesion at contact interface, immediately after mechanical action disrupts oxide films [18].

This experiment will be done in dry friction conditions

1.5. Aims of the work

The main objective of this work is to understand friction and wear phenomena at the contact between stem and neck adapter subjected to fretting in modular hip prosthesis and to study the influence of input parameters such as the displacement amplitude, the contact pressure, the number of cycles and the surface roughness on the behaviour of output parameters as the coefficient of friction, the dissipated energy and the wear volume.

From the literature review presented it can be concluded that there is not information available about the influence of the direction of roughness in the wear volume and in the size of the scars, hence the need to review this issue.

The strategy chosen to conduct this study was to perform dry fretting tests that simulate what happens between the stem and the neck adapter in hip prosthesis

1.6. Structure

This section is intended to guide the reader through the dissertation by showing the main aspects of each chapter.

Chapter 1: Presents a brief introduction about the hip joint and describes the background and the present situation for hip prosthesis by showing some previous results in arthroplasty. Shows the main materials used and explains the fretting behaviour, describing its conditions and the influential parameters on the process. It also include a brief explanation of the friction and wear phenomena. Finally, the main objectives of this study and how the dissertation is divided by is described.

Chapter 2: Explains the fretting tests including the material and geometry of the specimens, the equipment and parameters used, as well as analysis methods.

Chapter 3: Provides the surface analysis for the different components used. Presents and discusses the results of the tests regarding to the influence of the input parameters on the output ones. Presents an analysis on the cracks and verifies some previous bibliography.

Chapter 4: Presents the summary of the main conclusions of the previous chapters and an overview on perspectives for this subject.

2. EXPERIMENTAL ANALYSIS

The model of hip prosthesis used in this study was XO Femoral Stems with modular neck from the company *SEM science et médecine,* established in France. An image of the real prosthesis is shown (Figure 2.1). The size of the components varies from patient to patient.

Figure 2.1. Prosthesis model used for this study: XO Femoral Stems with modular neck, SEM – Science et medicine [32].

This study is intended to analyse the taper junction between the stem and the neck adapter (both made of Ti6Al4V) with the purpose of improving the design. For that, fretting tests with a cylinder on flat configuration were an option. The cylinder, that remains still, represents the stem and the flat, in oscillatory motion, represents the neck adapter. The extent of fretting damage depends on a combination of several factors, such as frequency, number of cycles, applied load, contact pressure and finally, roughness. A more detailed approach of the surfaces of the neck adapter and the stem is going to be presented in the next chapter.

2.1. Material used – Ti6Al4V

Titanium and its alloys are the most commonly materials used in the industry of biomedical implants and aerospace applications. Its high biological compatibility associated with the mechanical properties makes titanium alloys the base material that best suits the orthopaedic prostheses. However, there has been a great concern to improve the titanium alloy so that the replacement of organic elements last longer periods of time and with less surgical revisions than the materials used nowadays. For this purpose, it is being studied the possibility of introduction new alloys with properties closest to the human bone, without compromising the biological performance. For instance, the alloy Ti6Al7Nb where the element Vanadium, which demonstrated to be cytotoxic when isolated, is replaced by Niobium [33].

The titanium alloy used in this experiment was Ti6Al4V, according with NF EN ISO 5832-3. The most important features about this material are the fact that it has an excellent biocompatibility, not reacting with the human body, it has an extraordinary corrosion resistance and the ability to withstand extreme temperatures. Their composition is shown in Table 2.1.

Table 2.1. Microstructure of Ti6Al4V.

Component	Wt. %
Al	6
Fe	Max. 0,25
O	Max. 0,20
Ti	90
V	4

The microstructure shall be a fine dispersion of the alpha and beta phases resulting from processing in the alpha plus beta field [34].

Ti6Al4V has a value of the Young's modulus of approximately 110 GPa, a Poisson ratio of 0,35 [35] and a Yield strength 0,02% of around 820 MPa.

2.2. Testing conditions

2.2.1.   Geometry of the specimens

For this experiment, it was used a flat with two different directions of roughness and a cylinder. The flat represents the neck adapter and the cylinder represents the stem. The dimensions of the components are represented in the Figure 2.2.
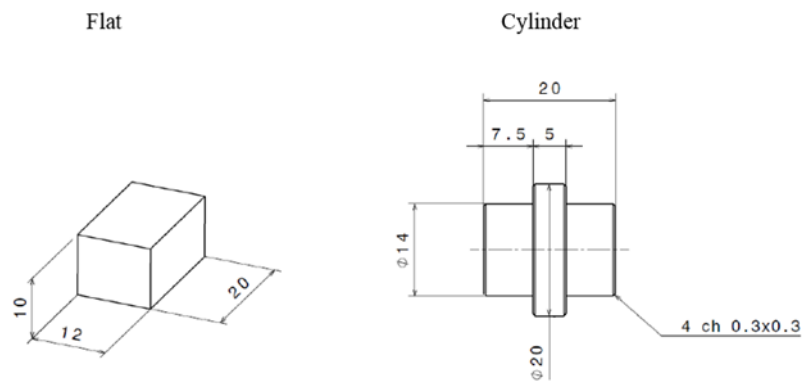
Figure 2.2. Illustration of the specimens [19].

2.2.2.   Fretting test – Equipment

The first step in carrying out the tests was to prepare the samples. This step relies basically in the cleaning of the surface to remove any residue, fat or particles that could affect the test. All samples were cleaned thoroughly with acetone then were in a bath of acetone followed by a bath of ethanol, both for 10 minutes.

The equipment used to perform the test was a fretting set-up based on a MTS tension-compression hydraulic machine and a MTS extensometer placed next to the contact in order to reach the various fretting regimes (gross, partial or mixed slip regime) and to limit the influence of the apparatus compliance. This allows setting the displacement between the flat and the cylinder [31].

The following sketch (Figure 2.3) represents the assembly of the tests. A more detailed approach of the equipment used is presented in Annex B.
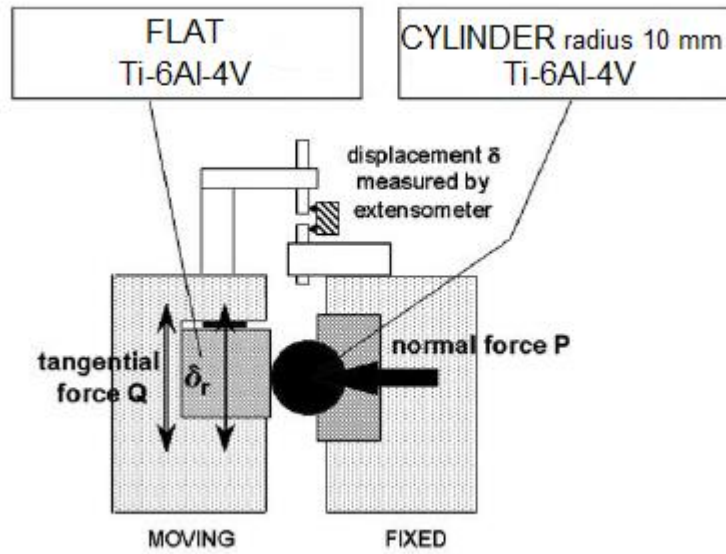
Figure 2.3. Sketch of the fretting wear rig used in this study [19].

For each test, the cylinder that remains fixed, and the flat that will be in motion should be as aligned as possible (Figure 2.4). After this assembly, the normal force that is intended is manually imposed, the cyclic sinusoidal displacement is then applied to generate an alternating tangential load Q on the contact and the remaining input parameters are entered into the software. Note that a displacement of δ^* means an amplitude from $-\delta^*$ to $+\delta^*$.

Figure 2.4. Flat on cylinder contact and direction of motion.

For selected cycle numbers during a fretting test, the displacement amplitude δ^*, the normal force P and the tangential force Q are recorded. This enables to plot the fretting loop $Q - \delta$ for the selected cycles (Figure 1.10 and Figure 1.11).

Input parameters:

- Normal force, P

- Displacement amplitude, δ^*

- Number of cycles, N_c

Output parameters:

- Fretting loop

- Coefficient of friction, μ

- Dissipated energy, E_d

2.3. Parameters used in the tests

The parameters used were chosen according to the bibliography presented in chapter 1.

Environment: The fretting tests were performed at room temperature and in dry conditions, which means that the materials are being tested under more severe conditions than in reality.

Frequency: Besides the fact that the average frequency of human walking is 1 Hz [22], the frequency was fixed at 5 Hz, in order to do the largest possible number of tests.

Number of cycles: In order to study the evolution of wear and cracking with the number of cycles it was chosen to run tests of 50.000, 100.000, 250.000 and 1.000.000 cycles to study the evolution of wear and cracking with the number of cycles.

Note that 50 cycles were added in each test in order to nullify the probability of not making up all the desired cycles, given a discrepancy between the software and the device connected to the machine.

Contact pressure/ Normal force: Due to the bibliography and from the conditions imposed by CETIM, it was chosen three values of contact pressure, 316, 490 and 632 MPa. Since the input value is the normal force, there was the need to carry out one iteration using Hertz's theory, so that the value is adjusted. The calculations can be found in Appendix A.

Displacement amplitude: In order to analyse wear and cracks and taking into account previous studies made by CETIM [25] it was decided to run tests of ±20, ±40 and ±70 μm. Later, for a more detailed analysis about the limits of values for the occurrence of cracks, it was imposed new conditions of ±8 and ±30 μm.

Note that, the value measured by the extensometer is not the accurate value of sliding amplitude at the interface since it has to be taken into account the elasticity of the contact, the samples and the samples holders.

Roughness: One of the main objectives of this work is to verify if roughness has an effect on fretting behaviour. In order to improve the contact between the neck adapter and the stem contact, were performed tests with two roughness directions; normal direction, i.e. perpendicular to the sliding direction and transversal. The Figure 2.5 shows how the contact between the two different types of flat and the cylinder is made.
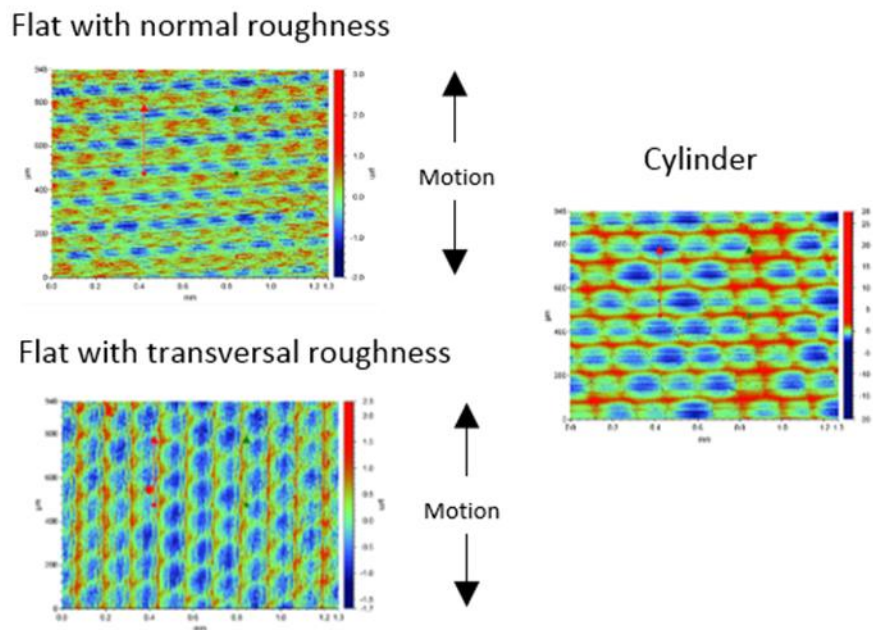
Figure 2.5. Images of the surfaces of the different components seen by interferometer. Size of each image: 1mm by 1mm. Representation of the contact of the surfaces of the flat with normal roughness and flat with transversal roughness with the cylinder. Representation of the direction of motion.

Table 2.2. Parameters chosen to perform the tests.

N_c	p_0 (Mpa)	P (N)	δ^* (µm)	Roughness
50.000 100.000 250.000	316 490 632	250 600 1000	8 20 30 40 70	Normal Transversal

The Table 2.2 presents the values used to perform the tests.

During this study were conducted 99 tests, 25 of which were not taken into account due to errors and crashes in the system.

2.4. Analysing techniques

During this work, different techniques were used for the evaluation and preparation of the samples.

Before performing the fretting tests, a study of the surface for the different parts was done using the interferometer.

After conducting the tests, it was performed a careful analysis about the scars; for the first step, the samples were inspected using the digital microscopy and the profilometer.

It follows a brief explanation about each technique used in the analysis.

Bruker interferometer (Figure 2.6)**:** Measurement method based on the principle of the interference of waves (in this case light), i.e., by using two light beams (usually by splitting one beam into two) an interference pattern is formed when these two beams overlap. Because the wavelength of the visible light is very short, small changes in the differences in the optical paths (distance travelled) between the two beams can be detected (as these differences will produce noticeable changes in the interference pattern) [36].

This technique was used to measure the surface of the different components, section 2.2.
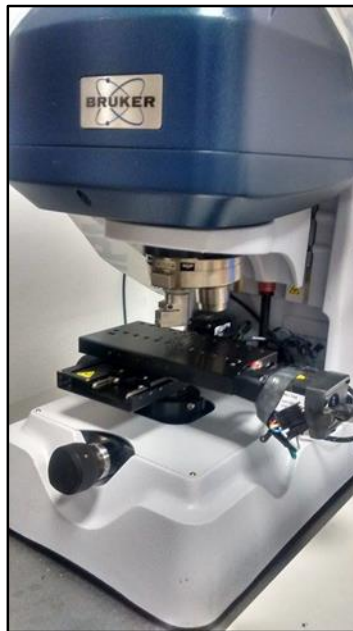
Figure 2.6. Bruker interferometer.

Digital Microscope, Keyence (VHX-1000): This microscope uses a camera to output a digital image to the monitor by a software in the computer.

This instrument was used to observe in large scale the surface of the different components used. It was also used to check the surface conditions and to measure the scars and cracks resulting from the fretting tests. The Figure 2.7 shows an image taken with the Keyence camera.
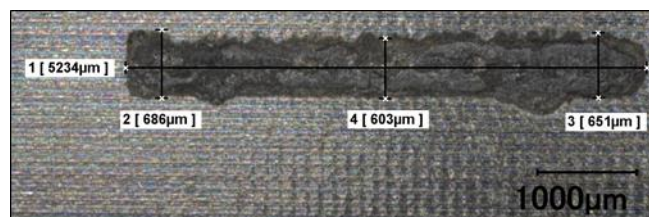
Figure 2.7. Image of a scar taken with keyence microscope with an amplification of 50x. Tests conditions: flat with normal roughness subjected to 600 N of normal force, ±20 μm of displacement amplitude and 100.000 cycles.

Two-dimensional contact profilometer (Surfascan, Somicronic - Figure 2.8)**:** Instrument used to measure the profile of a surface in order to quantify its roughness. The procedure consists in moving a diamond stylus, which is vertically in contact with the sample, laterally across the sample for a specified distance and specified contact force. A

profilometer can measure small surface variations in vertical stylus displacement as a function of position.

After having conducted a test and having a scar that can be analysed, this technique was used to measure the wear volume in the cylinder and in the flat. For this, it was set three cross-sections and in case of the flats it was even drawn a longitudinal profile. The Figure 2.9 shows the same profile for the flat and for the cylinder. Using the software, *dépouillement_profil*, it was possible to obtain the area of wear for each cross section. Finally, it was calculated the mean value of the measured wear surfaces multiplied by the total length of the scar, yielding the wear volume for the cylinder and for the flat. The sum of both is therefore the total wear volume for the test concerned.
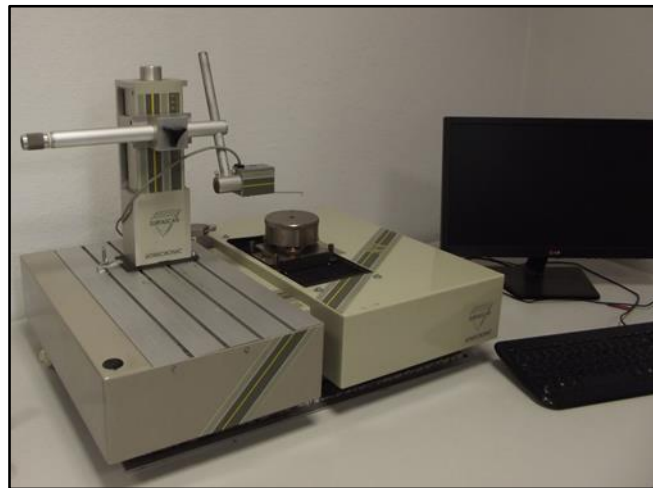
Figure 2.8. Two dimensional contact profilometer.
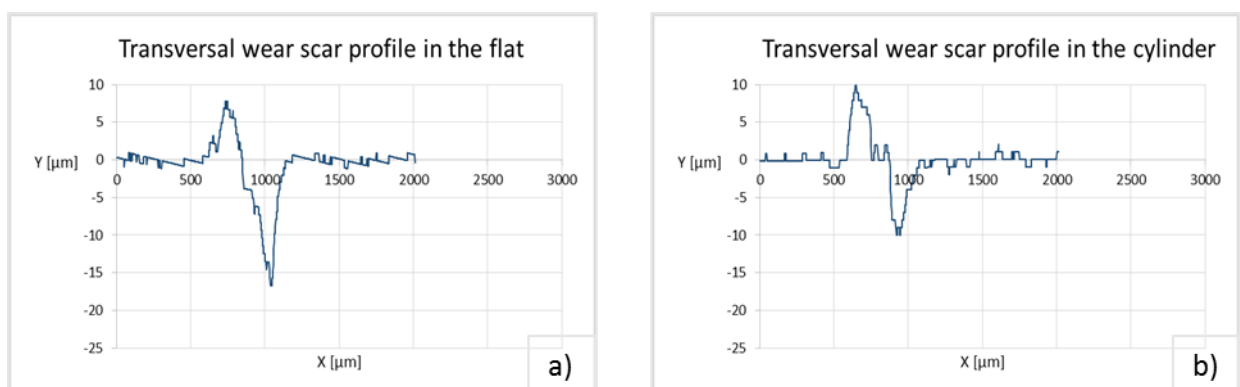
Figure 2.9. Profiles of a wear scar material. The wear surface below the reference line corresponds to the removal material, whereas, the surface above the reference line is due to adhesion phenomenon. a) Transversal wear scar in the flat. b) Transversal wear scar in the cylinder. Tests conditions: Normal roughness, 600 N of normal force, ±20 µm of displacement amplitude and 100.000 cycles.

Software for data analysis, (Trib-Fret LTDS): This software imports the data collected from the fretting test (h_0, E_d, P, Q, A, etc.), which allows tracing curves with different parameters and obtains the fretting log (Figure 2.10) for all cycles. Observing the fretting log it is possible to conclude about the regime of the test performed.
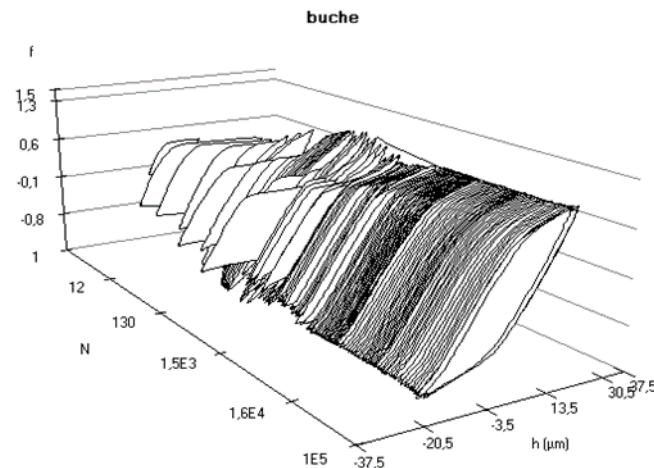
Figure 2.10. Fretting log for a test with a flat with normal roughness, subjected to a normal force of 600 N, a displacement amplitude of ±20 μm and 100.000 cycles.

After being drafted the full study of the resulting scars of fretting tests, it was carried out the analysis of cracks. Taking into consideration that for gross slip conditions, wear is the predominant feature with growth of a fretting crack being much less likely [15], at this stage it was only evaluated the tests on mixed and partial slip regime, that are the ones with a greater risk of crack nucleation [15].

Table 2.3. Parameters of the tests observed to be in partial and mixed slip regime.

Tests observed					
δ^* (μm)	8	20			30	40
P (N)	1000	250	600	1000	1000	600

Table 2.3 shows the parameters of the tests that were observed to be in partial and mixed slip regime. The next step is based in the following procedure for the preparation of the samples, in order to be able to analyse them using optical microscopy.

1º Cutting the sample

The sample was cut so as to observe the cross section of the scar. Cuts were made using Buehler, IsoMet™ 4000 Linear precision Saw with the disc MetAbraseTM, Abrasive Cut-Off Wheels for ferrous materials - 11-4207-010, Buehler (Figure 2.11).
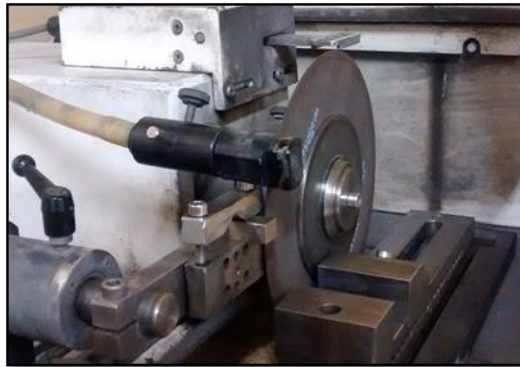
Figure 2.11. Cutting machine.

2º Involving the cut part in resin

After cutting, the samples were wrapped with Buelher TransOptic 20-3400-080 resin, using Buehler, Simplimet 1000 (Figure 2.12), Automatic mounting press, so that they can be polished efficiently.
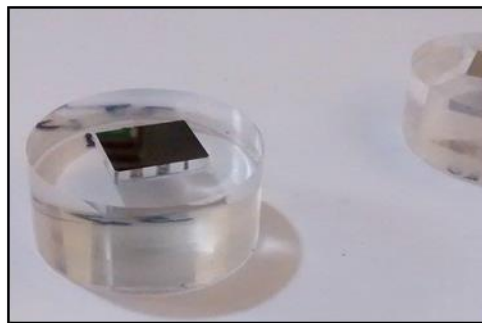
Figure 2.12. Sample in resin.

3º Polishing the sample

This step is very important because if not properly done it is not possible to observe and distinguish the cracks. For this, it was used the polishing machine Mecapol P220U – Presi; for each sample the polishing was done with three different types of abrasive

discs, made of silicon carbide (P1200, P2400 and P4000) and one synthetic cloth that was used with 3 µm Diamond compounds.

4º Analysing of the cracks in electronic microscope

Finally, the processed samples were analysed in the Keyence microscope. The Figure 2.13 represents a transversal wear scar. For a more detailed approach of the cracks, it was used higher amplifications.

Figure 2.13. Image of a transversal wear scar taken by Keyence microscope with an amplification of 300x Test conditions: flat with normal roughness subjected to 600 N of normal force, a displacement amplitude of ±20 µm and 100.000 cycles.

3. RESULTS AND DISCUSSION

The main objective of this dissertation was to understand friction and wear phenomenon at the contact between the stem and the neck adapter in a modular hip prosthesis. For this purpose it was necessary to know about the evolution between some parameters.

Then, it follows the demonstration of results. It begins with the characterization of the surface for each of the constituents under study. Then it is demonstrated some results for tests using the aforementioned techniques. Third, it was performed an analysis about friction and dissipated energy followed by an analysis about wear. Finally, the results for the study of the cracks are presented.

3.1. Surface characterization

With the purpose of ascertaining the conformity of the results between the test samples and hip joint prosthesis, a surface analysis was carried out resorting to interferometry technique.

Three roughness criteria were assessed (S_a, S_{sk} and S_{ku}) the surface cross hatch, to inquire about the anisotropy of the material; an image of the surface, that has size enough for the values to be representative (approximately 1mm by 1mm); and the graphic that relates the volume with the relative height where a higher plan was placed on the surface and went down until it reached the base of the profile.

It was expected that all the components were anisotropic and the stem, the plane with normal roughness, the cylinder and the neck adapter show the same direction of rolling. As for the graphic of volume, all the components should have the same behaviour. Finally, in order to have a representative results, the values of surface roughness of the samples must be similar to the one that they represent in reality, i.e. cylinder for stem and flat samples for neck adapter.
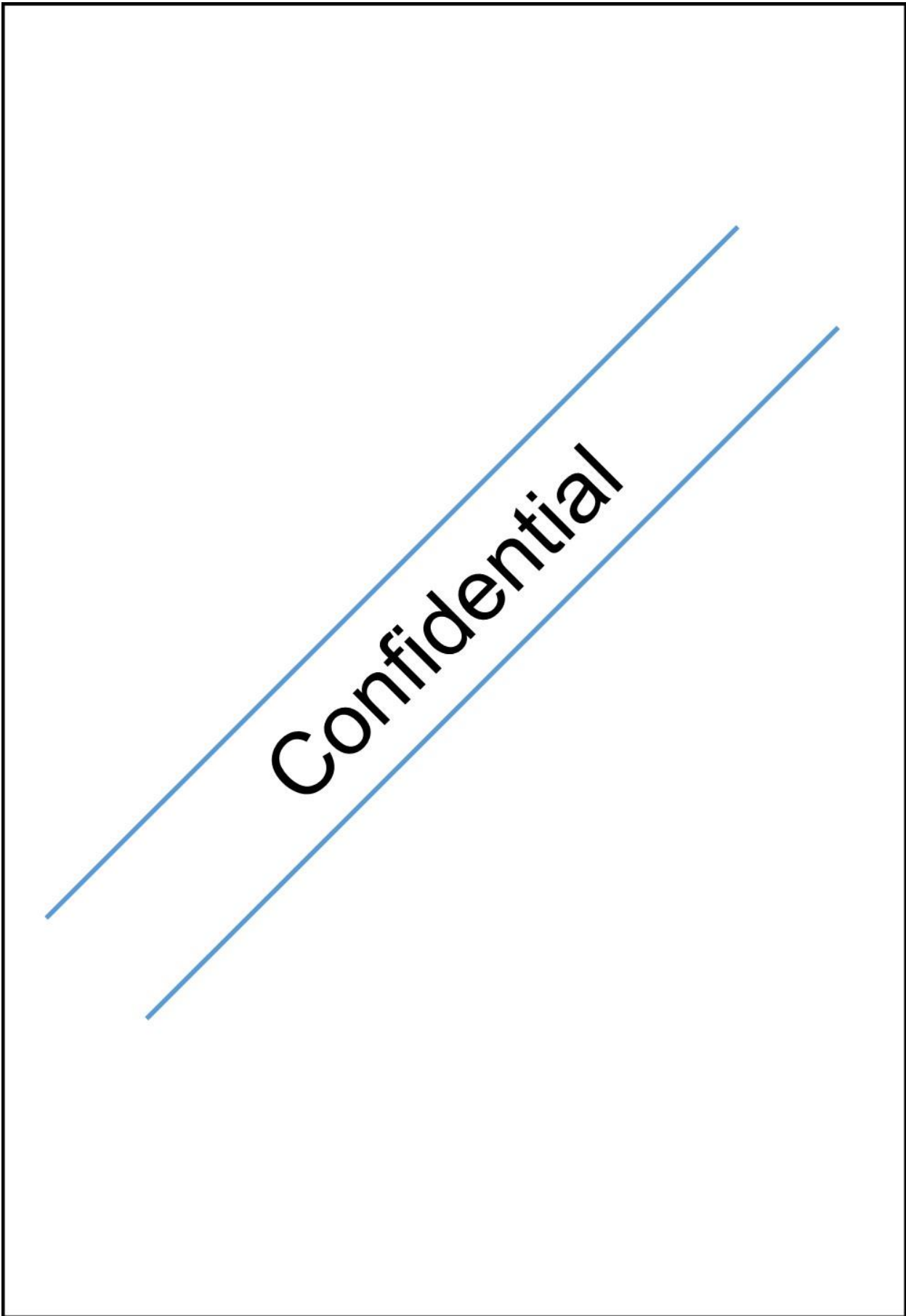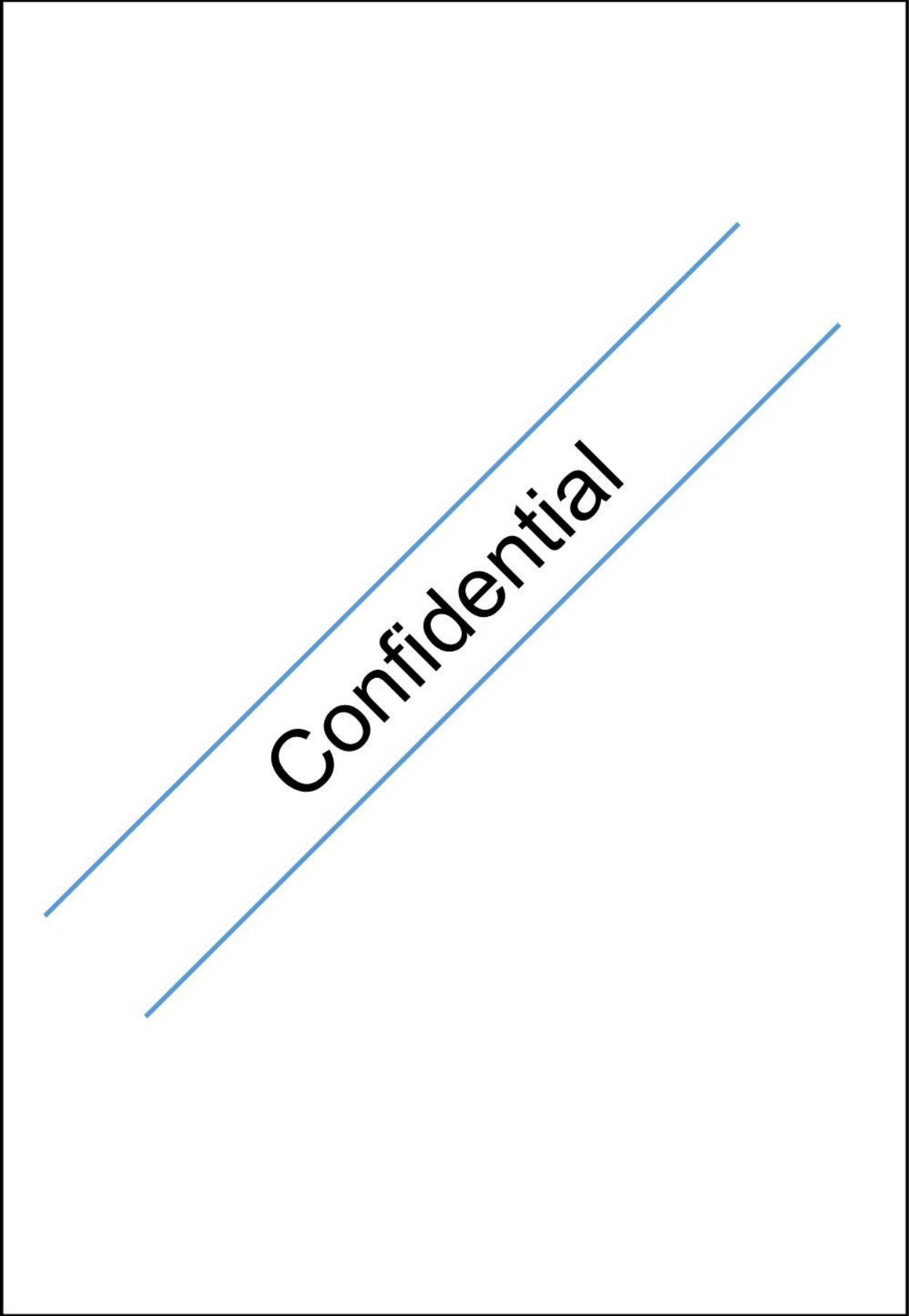
Confidential
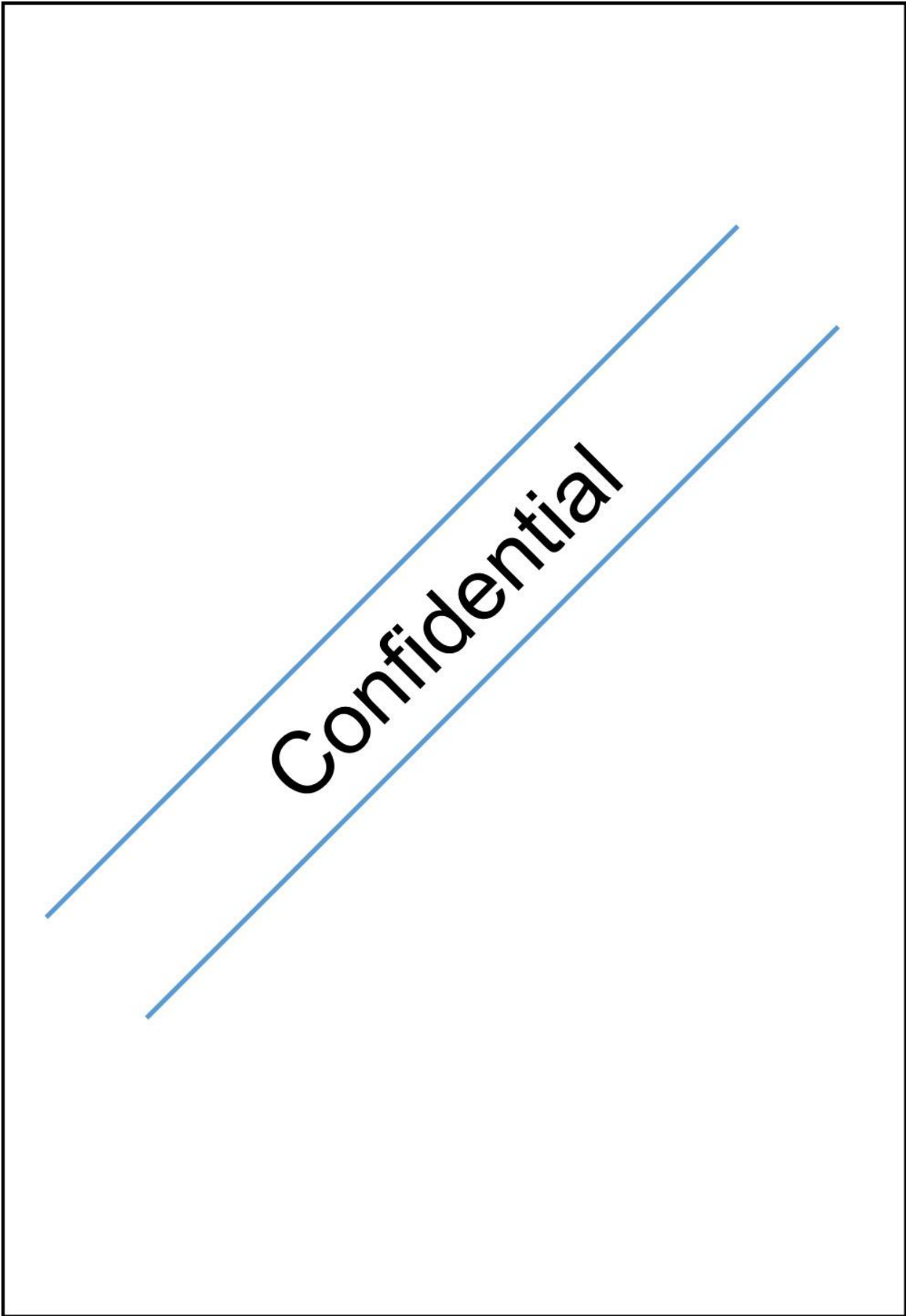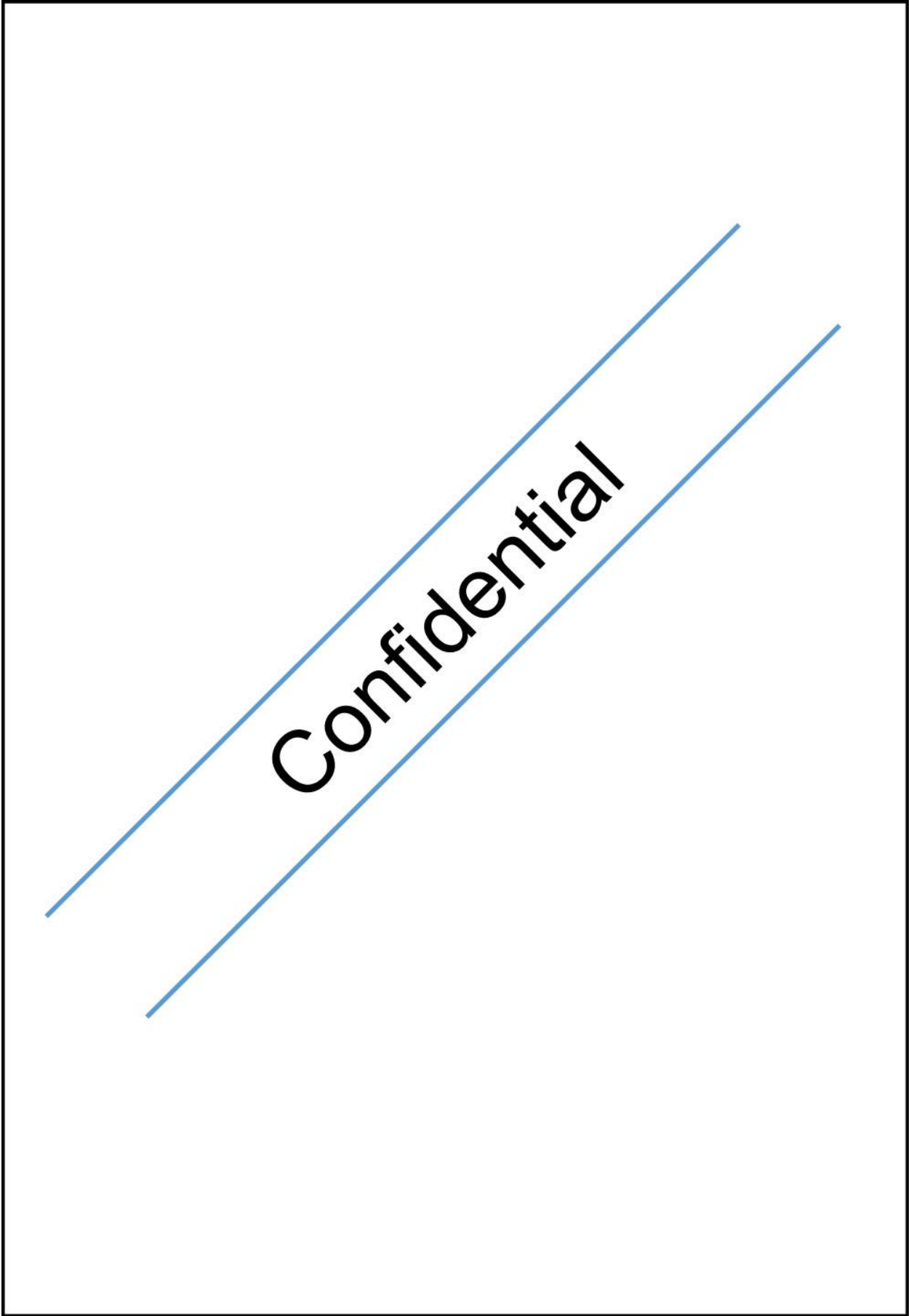
Confidential
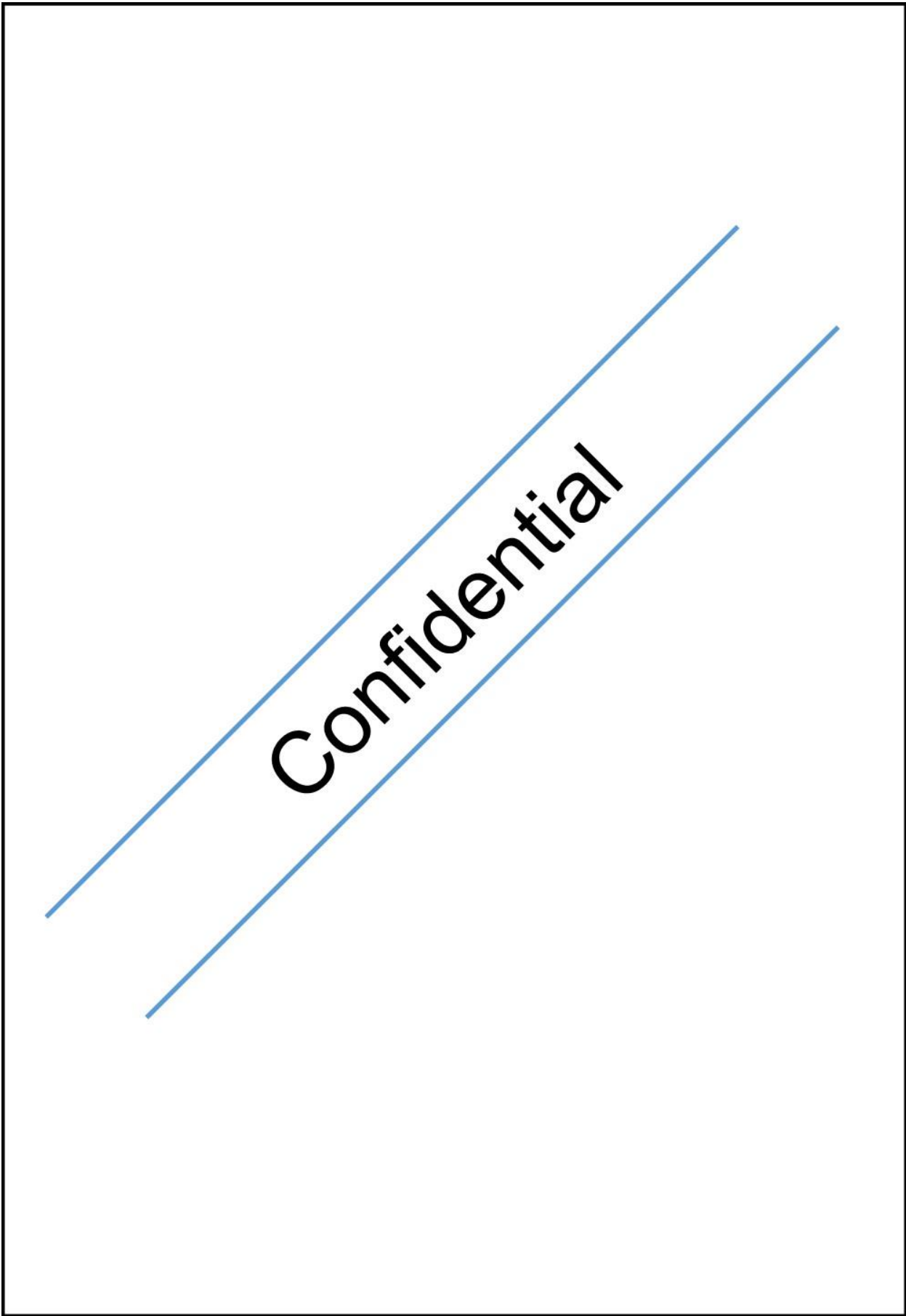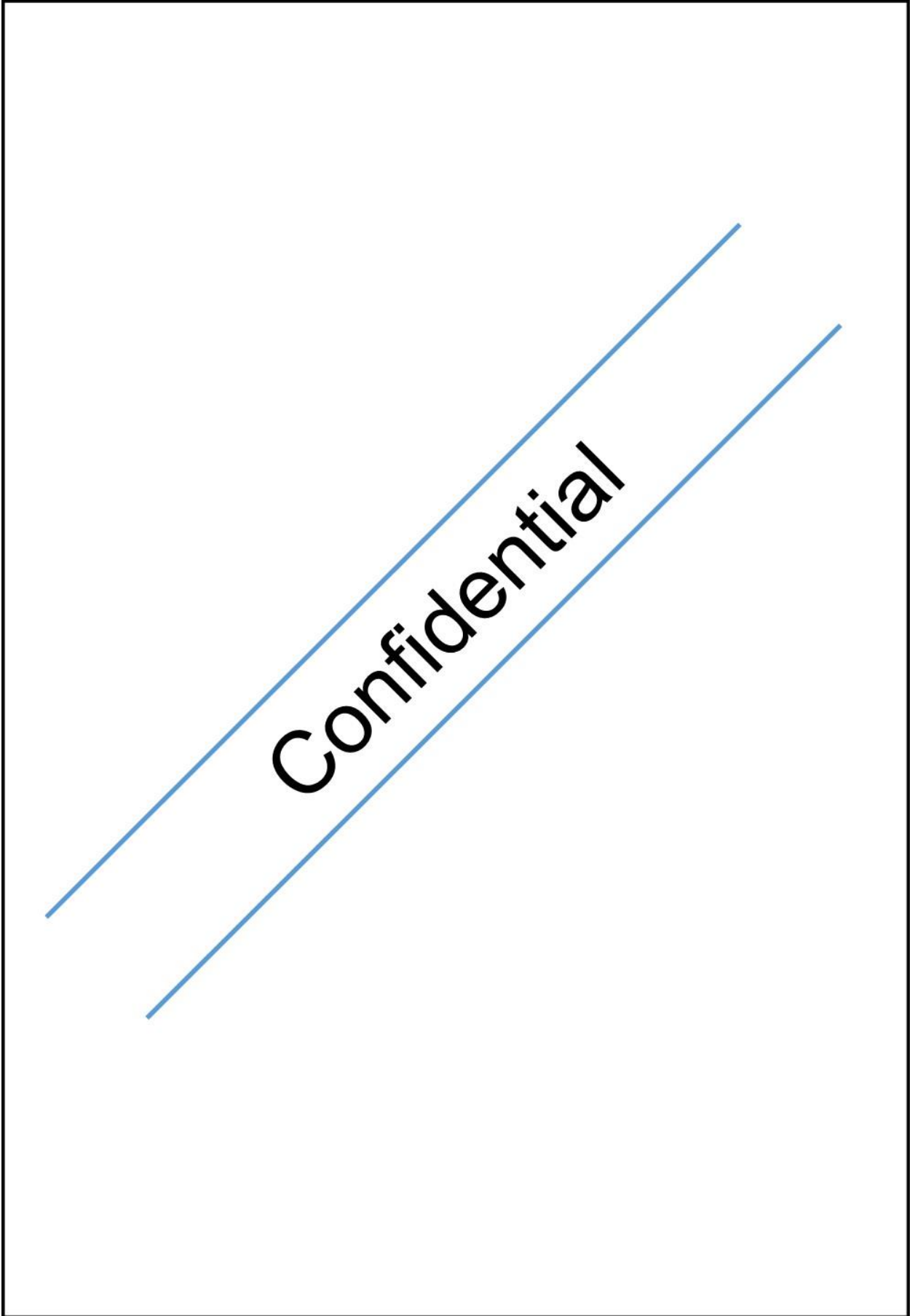
Confidential
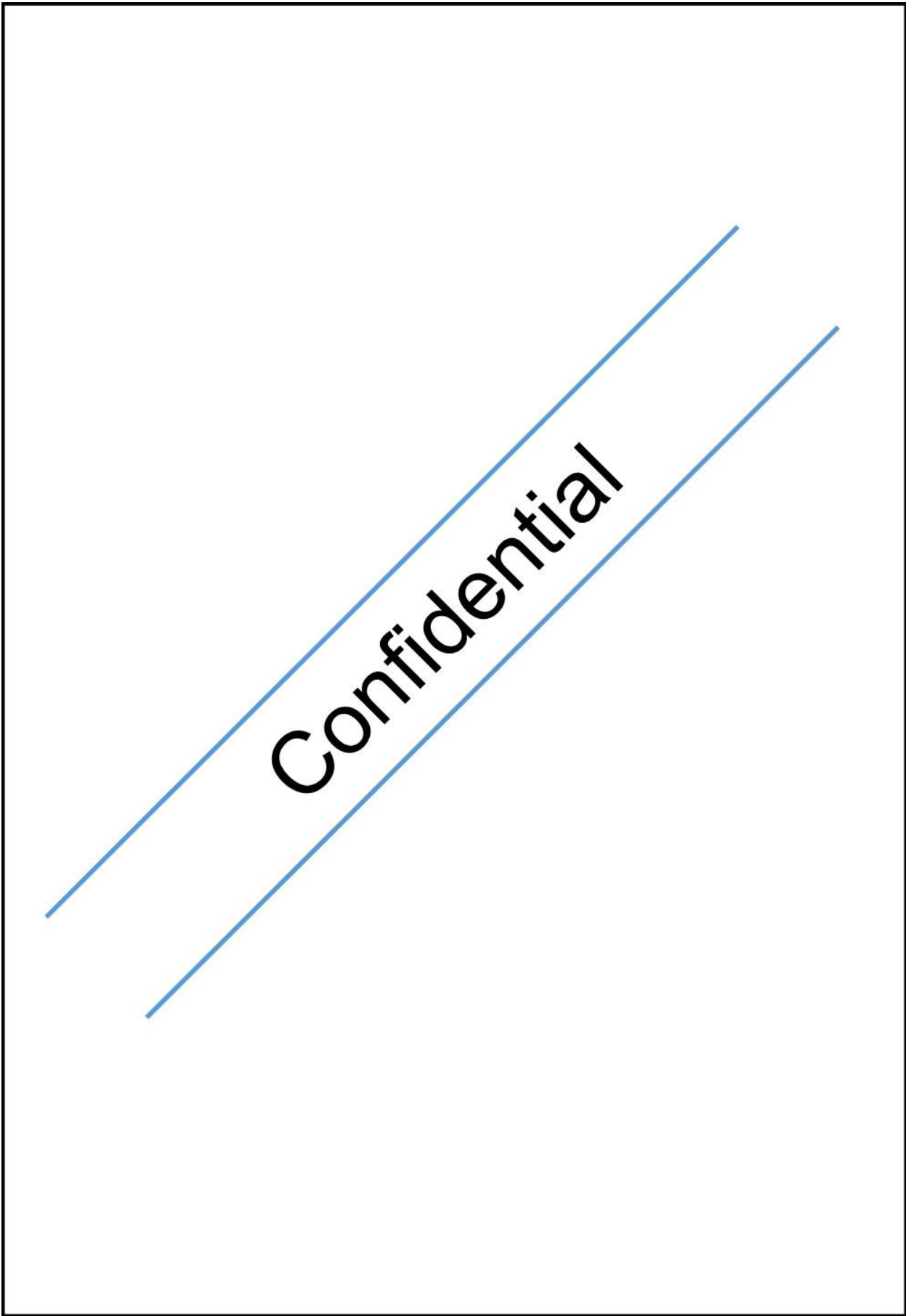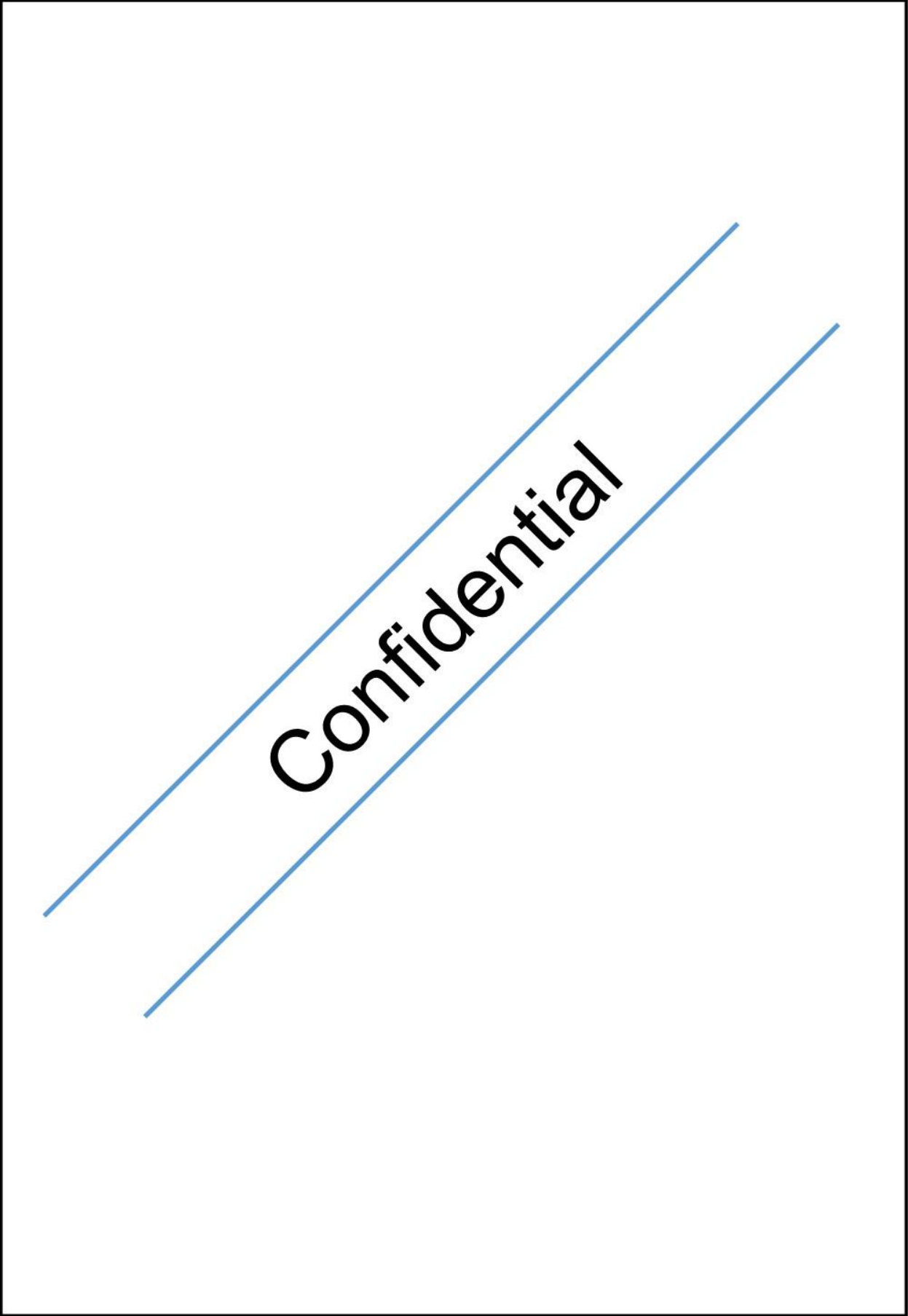
Confidential

Confidential
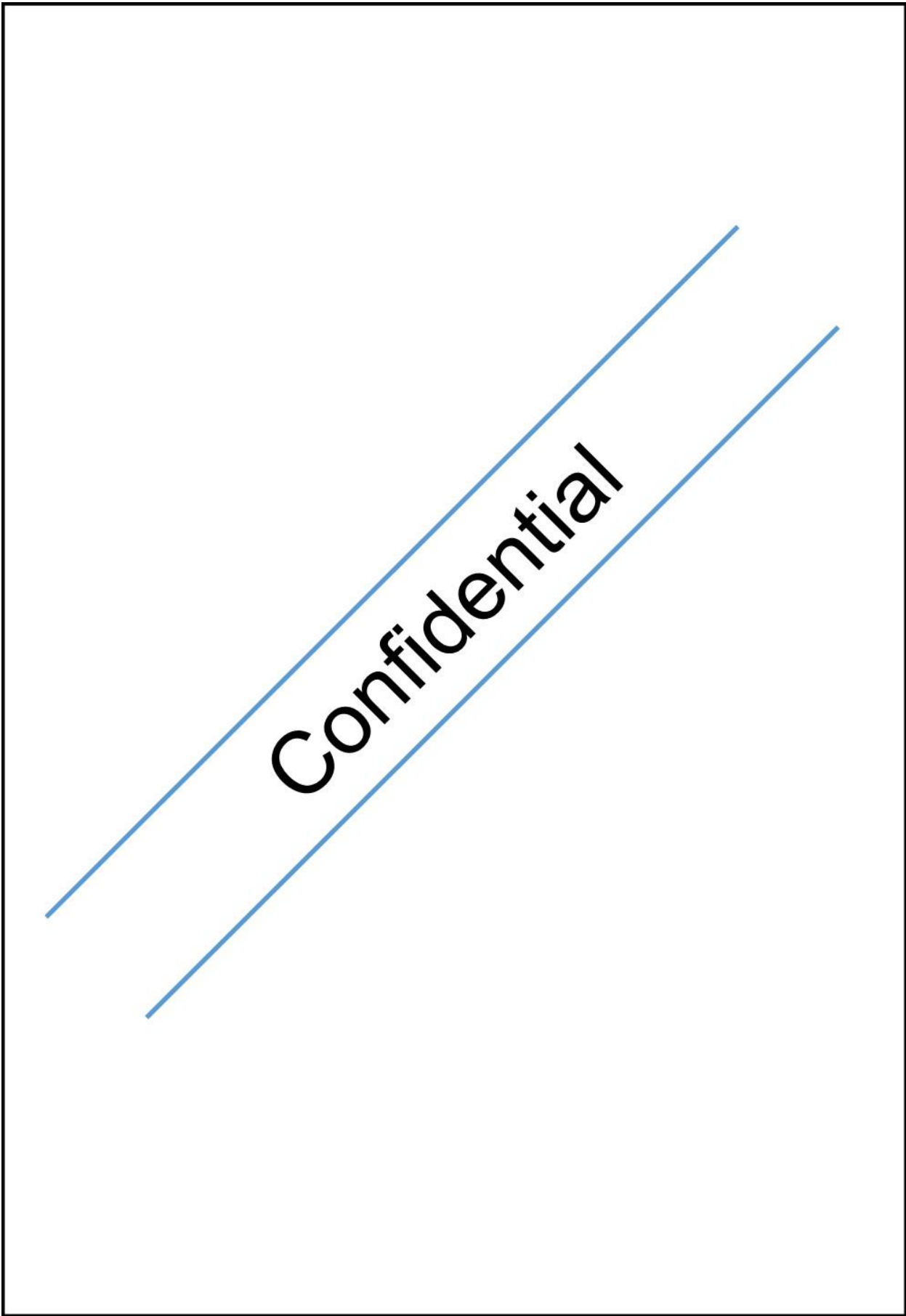
3.2. Analysis of selected tests

After running the fretting tests, the results were analyzed using techniques already described in section 2.4.

Next, an overview about the results of three cases with different parameters will be presented. It was chosen one test with a stable log, another one not stable, where the log varies over time, and the last one is representative of what normally happens in partial slip regime with visible cracks.

- Flat with normal roughness, 600 N of normal force, displacement amplitude of ±40 μm and 50.000 cycles

Figure 3.21. Image of a scar taken with keyence microscope with an amplification of 50x. Tests conditions: flat with normal roughness subjected to 600 N of normal force, ±40 μm of displacement amplitude and 50.000 cycles.

Figure 3.22. Fretting log for a test with a flat with normal roughness, subjected to a normal force of 600 N, a displacement amplitude of ±40 μm and 50.000 cycles.

Figure 3.23. Image of a transversal wear scar taken by Keyence microscope with an amplification of 300x Test conditions: flat with normal roughness subjected to 600 N of normal force, a displacement amplitude of ±40 µm and 50.000 cycles.
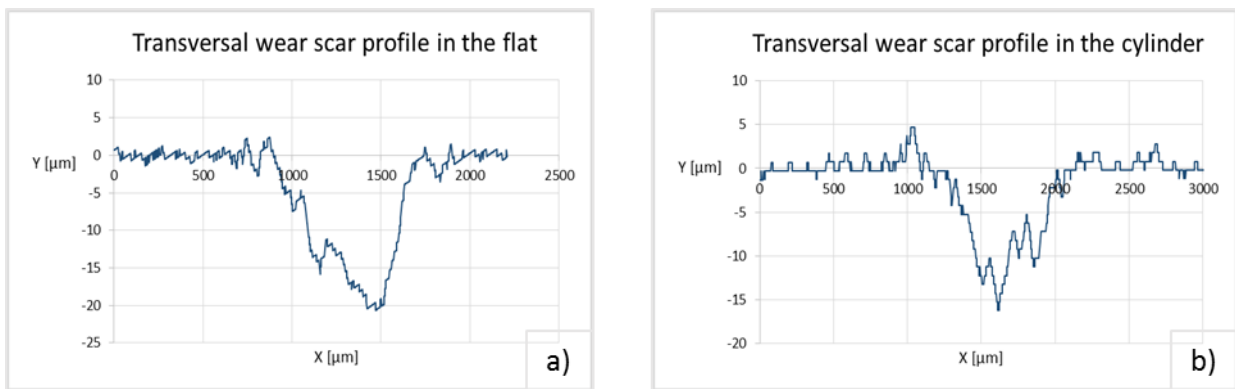
Figure 3.24. Profiles of a wear scar material. The wear surface below the reference line corresponds to the removal material, whereas, the surface above the reference line is due to adhesion phenomenon. a) Transversal wear scar in the flat. b) Transversal wear scar in the cylinder. Tests conditions: Normal roughness, 600 N of normal force, ±40 µm of displacement amplitude and 50.000 cycles.
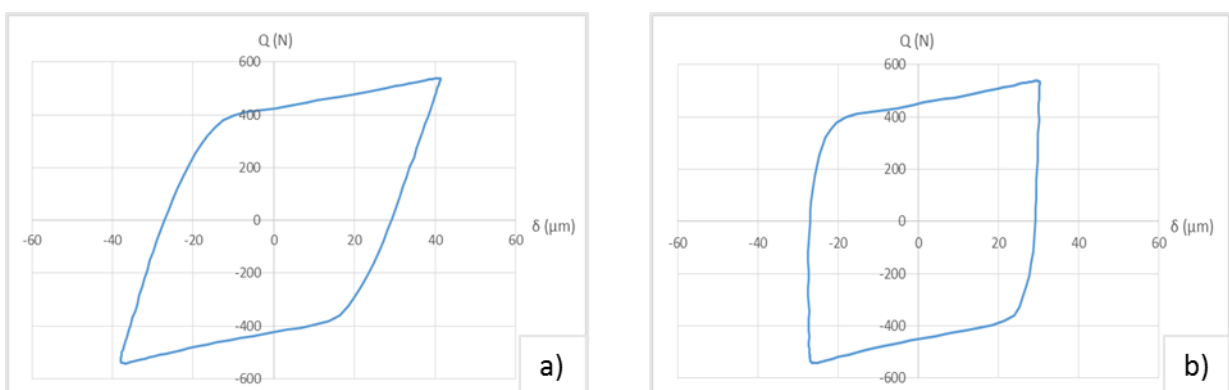
Figure 3.25. Fretting loop of the last cycle of the test. a) Without correction of the compliance. b) With correction of the compliance of the system.

RESULTS AND DISCUSSION

As the shape of the log is constant over the time this test is assumed as a stable one. Initially the data acquisition rate is higher, in order to analyse any running in effects, but over the time the periodicity increases, remaining constant after reaching a steady state regime.

Under these conditions, fretting loop is presented by a quasi-quadratic shape, which is typical for gross slip regime (Figure 3.22). For tests in gross slip regime, there is competition between the two wear mechanisms, i.e., although there is the occurrence of cracks, the extensive wear does not allows its growing.

In Figure 3.25 a) represented the fretting loop for the last cycle of the fretting test. Given the system deformation and after being corrected the compliance (Figure 3.25 b)), it was obtained the dissipated energy of the system from the calculation of the area of the loop.

Using tactile profilometer, it was drawn up three cross sections in the cylinder and in the flat, two of which are represented (Figure 3.24). The Figure 3.21 shows the location of the cross sections made in the scar of the flat. Its integration provides the wear volume. The length used was that one shown in Figure 3.21. One of the profiles of the cross section is shown in Figure 3.23.

- Flat with transversal roughness, 600 N of normal force, displacement amplitude of ±20 μm and 100.000 cycles
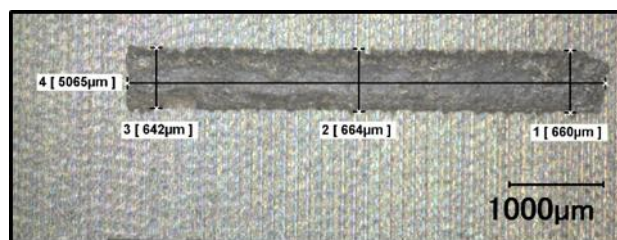
Figure 3.26. Image of a scar taken with keyence microscope with an amplification of 50x. Tests conditions: flat with transversal roughness subjected to 600 N of normal force, ±20 μm of displacement amplitude and 100.000 cycles.

Joana Filipa Jesus Pereira   45
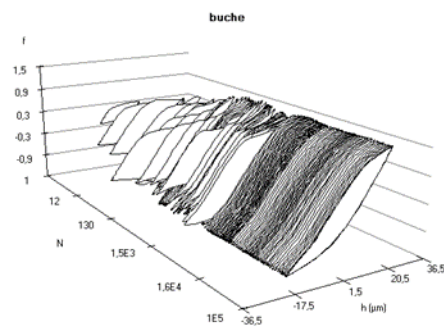
Figure 3.27. Fretting log for a test with a flat with transversal roughness, subjected to a normal force of 600 N, a displacement amplitude of ±20 μm and 100.000 cycles.
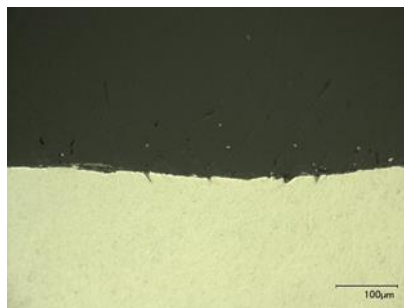
Figure 3.28. Image of a transversal wear scar taken by Keyence microscope with an amplification of 300x Test conditions: flat with transversal roughness subjected to 600 N of normal force, a displacement amplitude of ±20 μm and 100.000 cycles.

During most of the cycles, a partial slip regime occurs because a stable value of the tangential force was not reach.

This test has visible cracks and a stick zone in the central part of the contact (Figure 3.26).

It is observed that for the first cycles the fretting log is not constant (Figure 3.27), this is due to the fact that the outer surface may contain residues or fats that influence the progress of the trial. From the moment that this surface is worn, the log fretting starts to behave steadily.

Figure 3.26 provides an image of the scar and the location of the transversal cross sections (Figure 3.28), made in order to obtain the wear volume. The value for length is represented in the same image.

- Flat with normal roughness, 1000 N of normal force, displacement amplitude of ±30 μm and 50.000 cycles
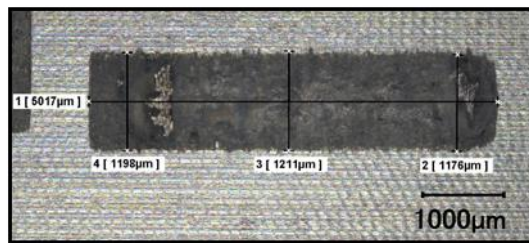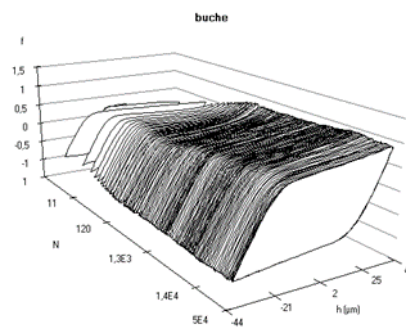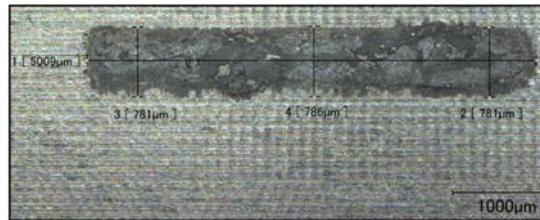

Figure 3.29. Image of a scar taken with keyence microscope with an amplification of 50x. Tests conditions: flat with normal roughness subjected to 1000 N of normal force, ±30 μm of displacement amplitude and 50.000 cycles.
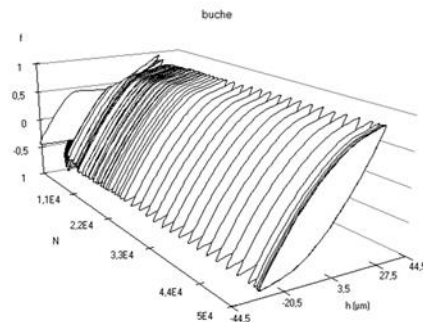
**Figure 3.30.** Fretting log for a test with a flat with normal roughness, subjected to a normal force of 1000 N, a displacement amplitude of ±30 μm and 50.000 cycles.
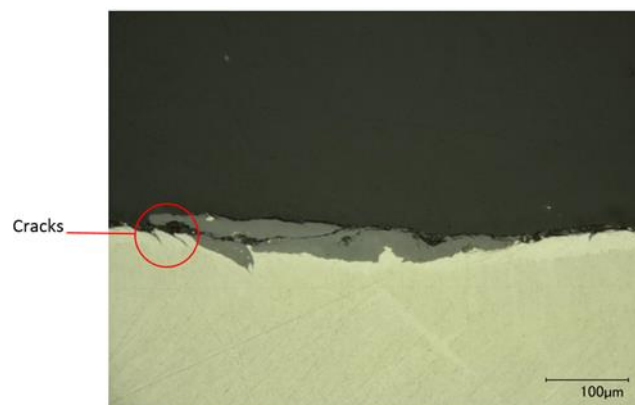
Figure 3.31. Image of a transversal wear scar taken by Keyence microscope with an amplification of 300x. Indication of the localization of the cracks. Test conditions: flat with normal roughness subjected to 1000 N of normal force, a displacement amplitude of ±30 μm and 50.000 cycles.

This test is in partial slip regime given the, almost perfect, elliptical shape of the log (Figure 3.30).

In Figure 3.31 it is possible to observe some cracks. For its analysis, it was taken into account the average value of the length of all the cracks observed for the same test. Besides the cracks, due to adhesion phenomenon and transfer of material, it is also visible a dark layer of oxides, called tribology transformed structure.

Figure 3.29 shows the scar and the location of the transversal cross sections, made in order to obtain the wear volume. The value for length is represented in the same image.

3.3. Analysis of friction and dissipated energy

One of the objectives of this dissertation is to analyse the influence of the input variables on the output ones. For such, it was necessary to study the variation of the parameters.

Below, lies the statement of results for tests with different characteristics.

As expected for each test, the friction coefficient had an initial rise due to the adhesion properties of titanium alloy [18].

The first parameter to be studied is the friction coefficient. As it was said before, for tests in partial slip the relation between the maximum tangential force Q^* and the normal force P, does not correspond to a coefficient of friction, therefore it is represented as Q^*/P [19].

The tests performed with 600 N and 250 N for a displacement amplitude of ±40 µm and ±70 µm are in gross slip regime, and the ones with a displacement amplitude of ±20 µm, due to the nature of the contact, are in a mixed slip regime. For a given normal force, number of cycles and displacement amplitude.

Because the number of cycles has not a significant change in the slip regimes, Table 3.2 summarizes the effect of the normal load and the displacement amplitude, allowing to conclude that partial slip was predominant for tests with high load and low displacement amplitude while the gross slip was more prone when the load is low and the displacement amplitude is high.

Table 3.2. Classification of the fretting regime obtain for each test, regarding the parameters use.

		P (N)		
		250	600	1000
δ^* (μm)	8	NT	NT	
	20			
	30	NT	NT	
	40			NT
	70			NT

Caption	
NT	Not Tested
	Tests in partial slip regime
	Tests in mixed slip regime
	Tests in gross slip regime

The following figures show the relation between the Q^*/P (Figure 3.34) or μ, in case of tests in GS (Figure 3.32 and Figure 3.33), with the number of cycles for each direction of roughness and normal force for different displacement amplitudes. Note that the values of the coefficient of friction were obtained with the average of the five last values recorded for each test.
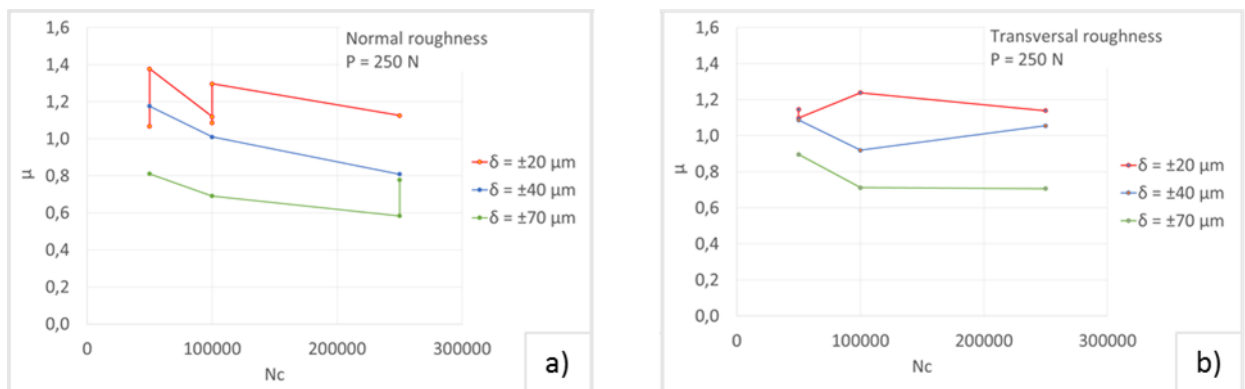
Figure 3.32. Relation between the coefficient of friction and the number of cycles for a normal force of 250 N and for a) Normal roughness and b).Transversal roughness.
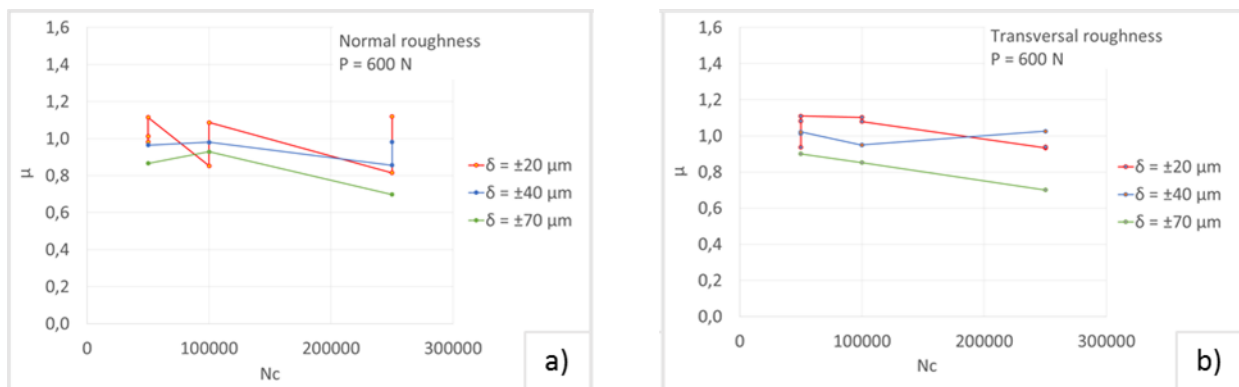
Figure 3.33. Relation between the coefficient of friction and the number of cycles for a normal force of 600 N and for a) Normal roughness and b).Transversal roughness.
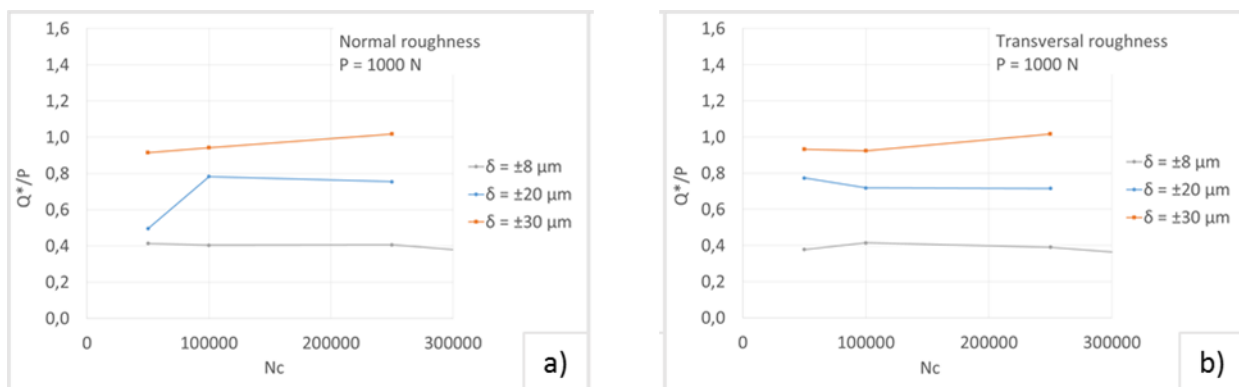
Figure 3.34. Relation between the ratio of the tangential force with the normal force and the number of cycles for a normal force of 1000 N and for a) Normal roughness and b).Transversal roughness.

As it is possible to see, friction coefficient is higher than the maximum presumed value, 1,0 [23] [24]. The obtained values are between 0,6 and 1,4. It is also possible to observe that there is no relation established between the increase in the number of cycles and the friction coefficient, neither significant differences between the two types of roughness nor for different normal force.

A different approach of the evolution of these same parameters was performed. In Figure 3.35 and in Figure 3.36 it is shown its evolution for each displacement amplitude for different normal forces and roughness. Note that NR refers to the tests performed with a flat with normal roughness, i.e. perpendicular to the sliding direction; TR means transversal roughness and it refers to the tests performed with the flat with the same direction of the sliding.
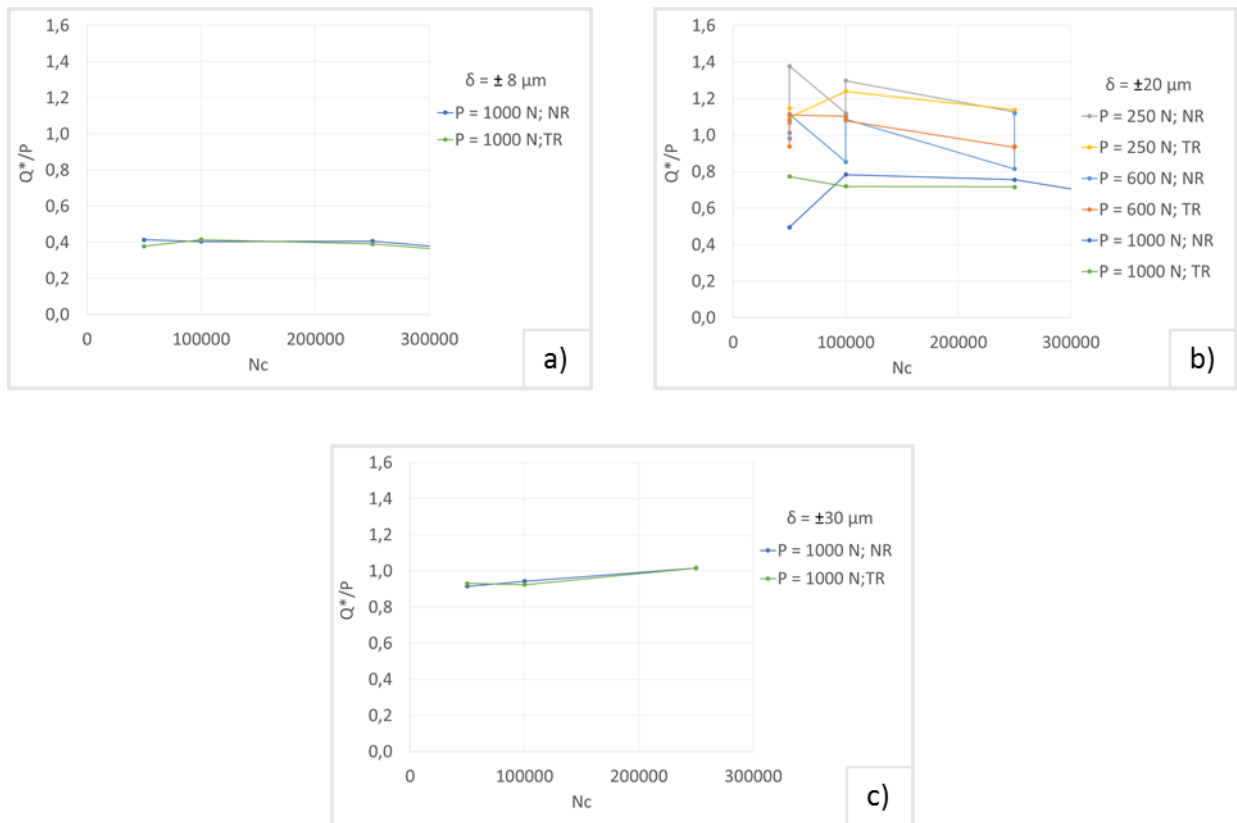
Figure 3.35. Evolution of the ratio between the tangencial force and the normal force with the number of cycles for a displacement amplitude of a) ±8 μm, b) ±20 μm and c) ±30 μm.
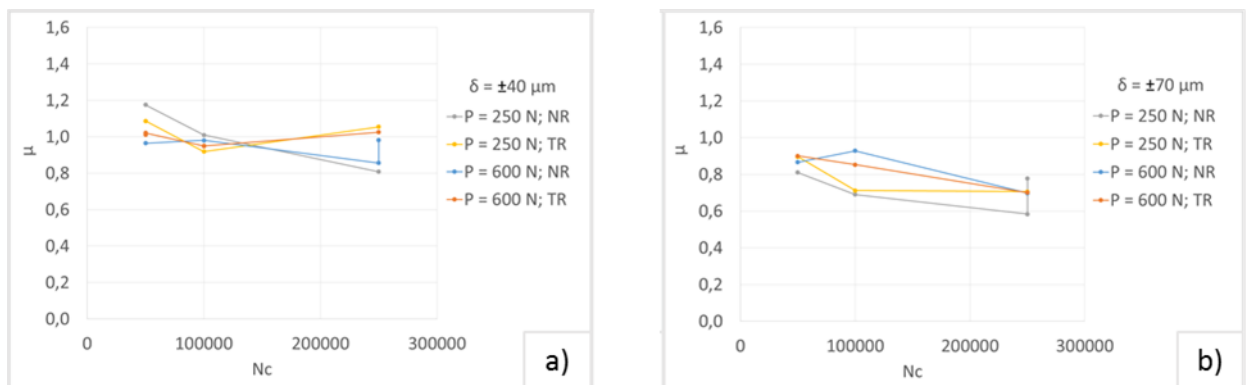
Figure 3.36. Evolution of the coefficient of friction with the number of cycles for a displacement amplitude of a) ±40 μm and b) ±70 μm.

It cannot be concluded that there is an evident relation between the displacement amplitude and the coefficient of friction.

The following parameter to be studied is the accumulated dissipated energy. This parameter allows to have an idea about the behaviour of the test, since it represents the area

of each fretting loop. It depends on the coefficient of friction, the displacement amplitude and the normal force.

The Figure 3.37, Figure 3.38 and Figure 3.39 show the evolution of the total amount of the dissipated energy with the number of cycles for different displacement amplitudes, normal force and roughness direction.
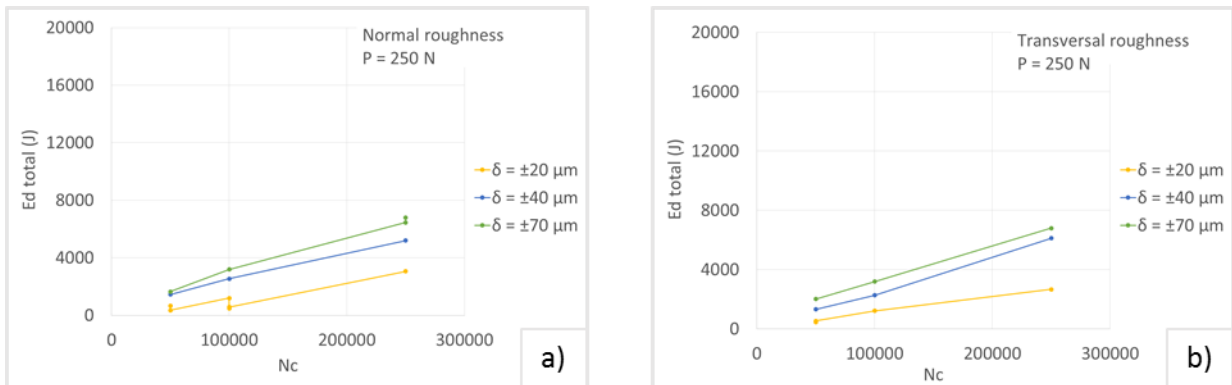
Figure 3.37. Evolution of the dissipated energy with the number of cycles for a normal force of 250 N and for a) Normal roughness and b) Transversal roughness.
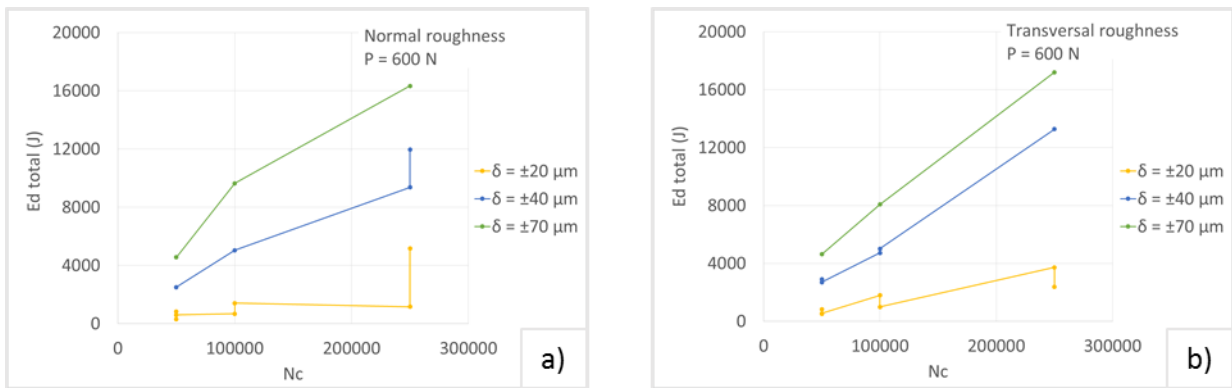
Figure 3.38. Evolution of the dissipated energy with the number of cycles for a normal force of 600 N and for a) Normal roughness and b) Transversal roughness.
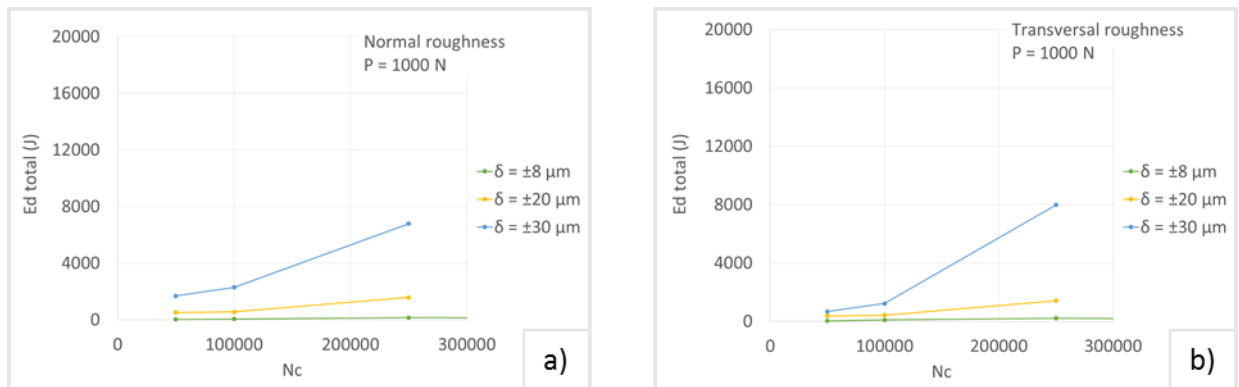
Figure 3.39. Evolution of the dissipated energy with the number of cycles for a normal force of 1000 N and for a) Normal roughness and b) Transversal roughness.

As expected, the maximum amount of dissipated energy is for the maximum displacement amplitude. Low dissipated energy is observed for tests in partial slip regime which are the ones with less wear and high rate of adhesion and transfer of material.

For the vast majority of cases and as expected, the dissipated energy increases with increasing number of cycles, the opposite phenomenon can be due to minor problems during the test assembly.

For the tests in gross and mixed slip regime, there is more energy dissipated for greater values of normal force. For $\delta = \pm 20$ μm there is no considerable differences in the evolution of the dissipated energy for the different values of normal force.

There is no significant differences between normal and transversal roughness.

3.4. Analysis of wear

The wear volume is an important parameter, since it gives a lot of information about the surface of the material. It is measured taking into account the worn surfaces on the flat and on the cylinder. In Figure 3.40 it is presented the evolution of the wear volume with the number of cycles for the different conditions.
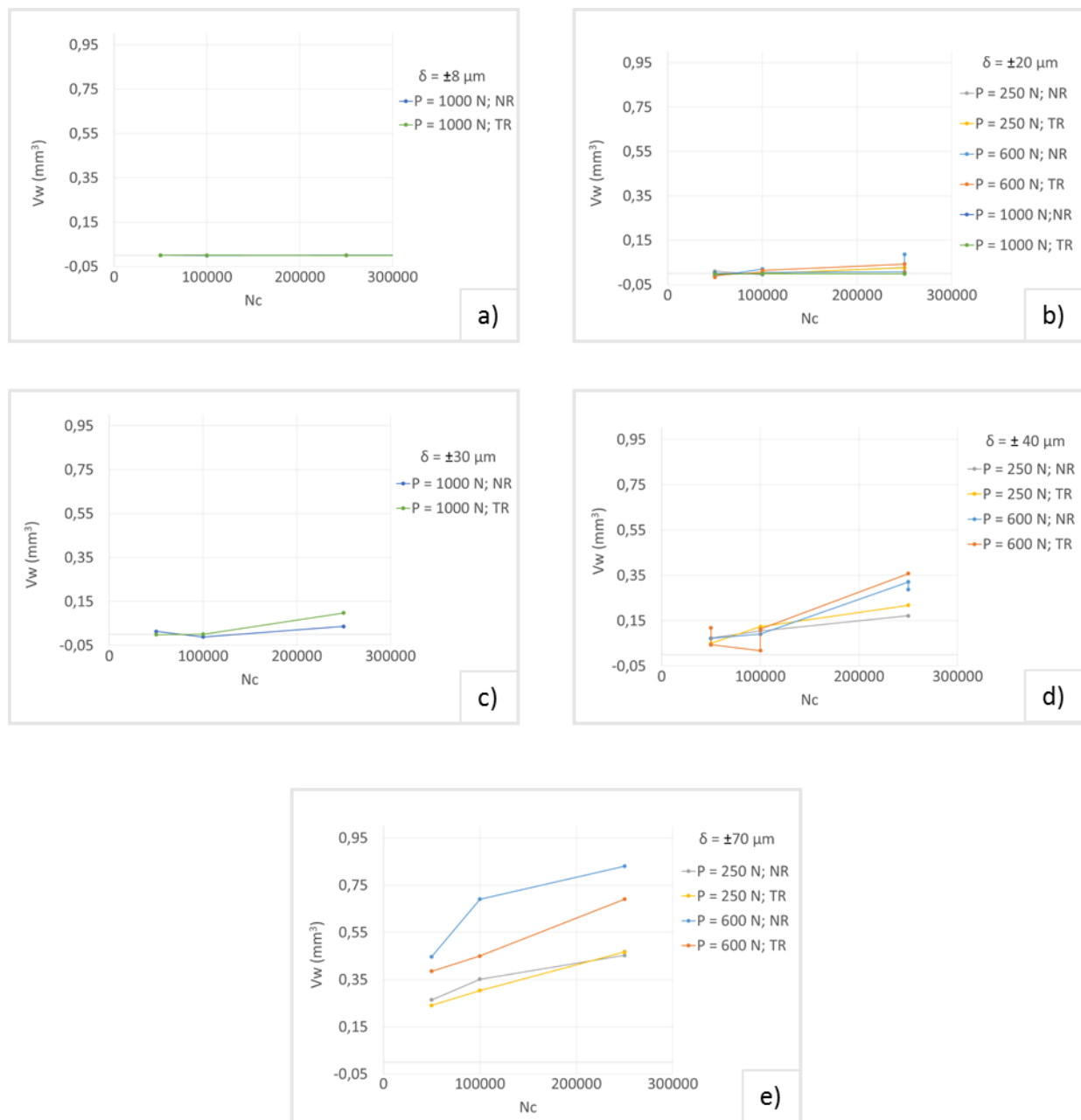
Figure 3.40. Evolution of the wear volume with the number of cycles for a displacement amplitude of a) ±8 μm, b) ±20 μm, c) ±30 μm, d) ±40 μm and e) ±70 μm.

The tests with a displacement amplitude of ±8 μm (in stick regime) have a very limited surface damage.

It can also be observed that the wear volume is higher for higher displacements. Furthermore, although it is not a linear evolution, the wear volume tends to increase with increasing number of cycles. It is not verified a clear relation between normal and transversal roughness.

The following graphics (Figure 3.41) show the evolution of the wear volume with the number of cycles but presented in different way than the previous ones, that allows to see how it progresses for the three different normal force.
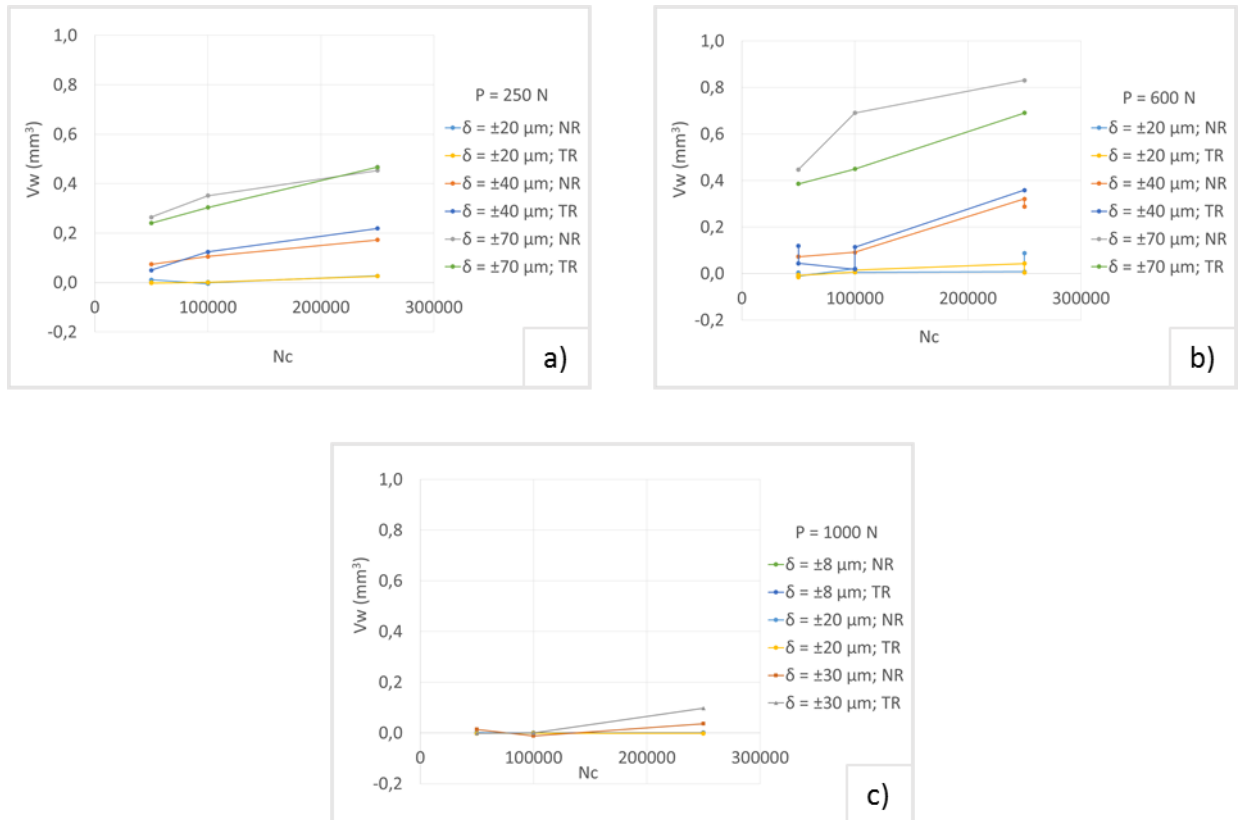
Figure 3.41. Evolution of the wear volume with the number of cycles for a normal force of a) 250 N, b) 600 N and c) 1000 N.

As expected for tests in partial slip regime the wear volume is much lower than for tests in gross and mixed slip regime, for instance, for $\delta = \pm70$ μm and $P = 600$ N, the wear volume is almost up to 8 times higher than the wear volume for $\delta = \pm20$ μm. It is verified that for the tests in gross slip regime there is a slight increase of the wear volume for higher normal force/ contact pressure.

It is not possible to assume that one type of roughness wear more than the other.

The connexion of the wear volume with the dissipated energy was also studied. Therefore, in Figure 3.42, Figure 3.43 and in Figure 3.44 it is presented the relation between these two factors for the different types of roughness and normal force.
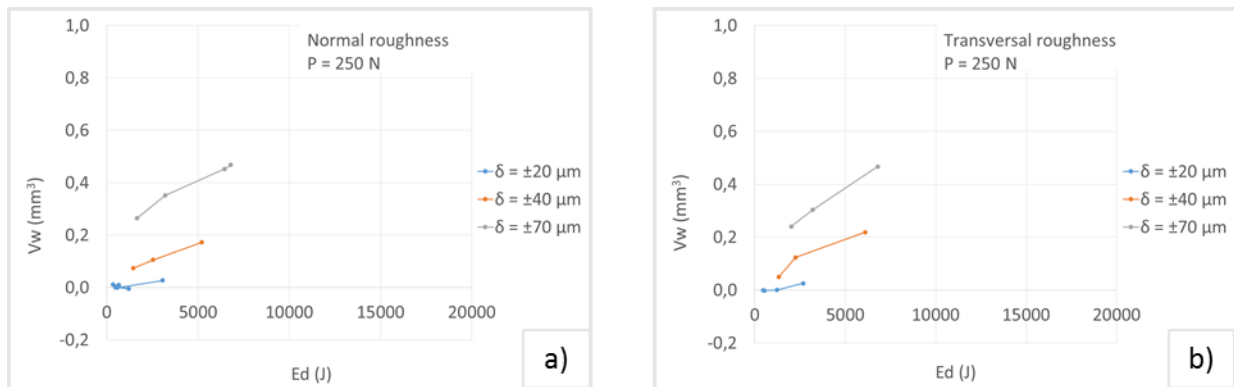
Figure 3.42. Evolution of the wear volume with the dissipated energy for a normal force of 250 N and a) Normal roughness and b) Transversal roughness.
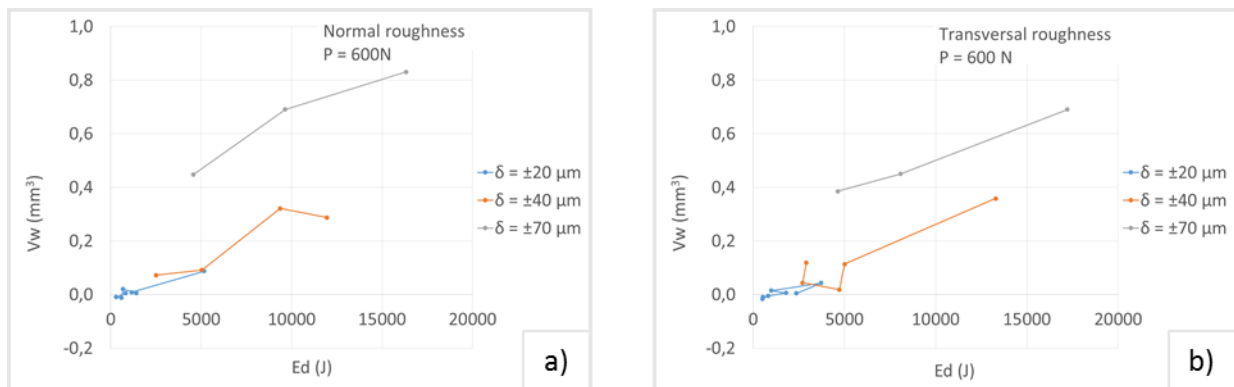
Figure 3.43. Evolution of the wear volume with the dissipated energy for a normal force of 600 N and a) Normal roughness and b) Transversal roughness.
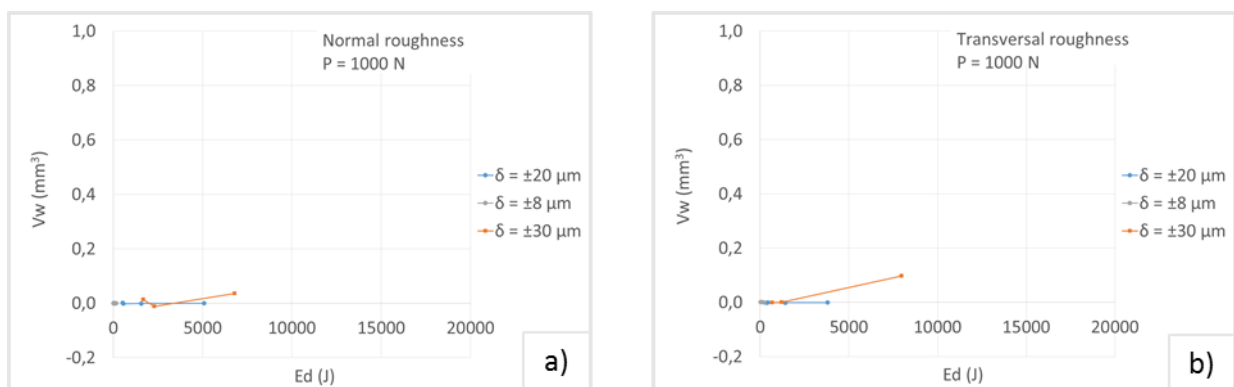
Figure 3.44. Evolution of the wear volume with the dissipated energy for a normal force of 1000 N and a) Normal roughness and b) Transversal roughness.

For lower loads, with increasing displacement amplitude the wear volume increases. Significant differences between the two different roughness are not observed.

The low values of dissipated energy and the discrepancy in the results of the tests in partial slip regime are due to adhesion and transfer phenomenon.

An extra evaluation was done in order to ascertain about the likeliness of each component (flat or cylinder) to wear. It relates the wear volume with the dissipated energy for the cylinder and for the flat. It was concluded that it cannot be admitted a relation between both the parameters. The results are shown is Appendix B.

Previous literature [31] assumes that wear evolution for titanium alloys can be normalized in a master curve. This evolution is a function of the wear volume with the dissipated energy multiplied by the displacement. According to this, the curve should have a linear behaviour. Thus, it was proceeded to the confirmation of this theory. Note that all tests were taken into consideration.

The Figure 3.45 a), presents the evolution of the wear volume with the dissipated energy, whereas Figure 3.45 b) presents the evolution of the wear volume with the product of the dissipated energy by the amplitude. Both with normal roughness.

Figure 3.45. Evolution of the wear volume with a) The dissipated energy and b) The product of the dissipated energy by the displacement. For tests with normal roughness.
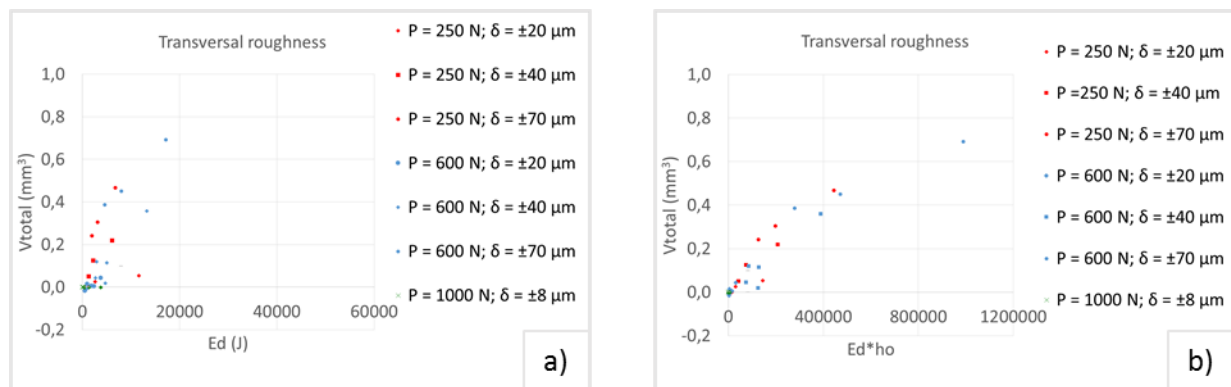
Figure 3.46. Evolution of the wear volume with a) The dissipated energy and b) The product of the dissipated energy by the displacement. For tests with transversal roughness.

For Figure 3.46 a) and b), it is related, respectively, the wear volume with the dissipated energy and the wear volume related with the product of the dissipated energy by the displacement. Both for transversal roughness.

It is possible to see that for Figure 3.45 a) and for Figure 3.46 a) it is not achieved a straight line, which means that the dissipated energy is not the only parameter for wear.

On the other hand, for theFigure 3.45 b) and Figure 3.46 b), with a high value of displacement amplitude, for the same dissipated energy, it will be more wear volume (for instance, figure b, $\delta = \pm 40$ μm and $P = 600$ N vs $\delta = \pm 70$ μm and $P = 250$ N). This is because, when there is high values of displacement amplitudes, it is easier for the debris to be ejected, generating more wear volume.

For a more detailed analysis, it was used a linear regression. With this technique it was possible to verify that the graphics that are based on the present theory (Figure 3.47 b) and Figure 3.48 b)) have a good correlation, with R^2 values close to 1, whereas the others (Figure 3.47a) and Figure 3.48 a)) have a poor correlation.
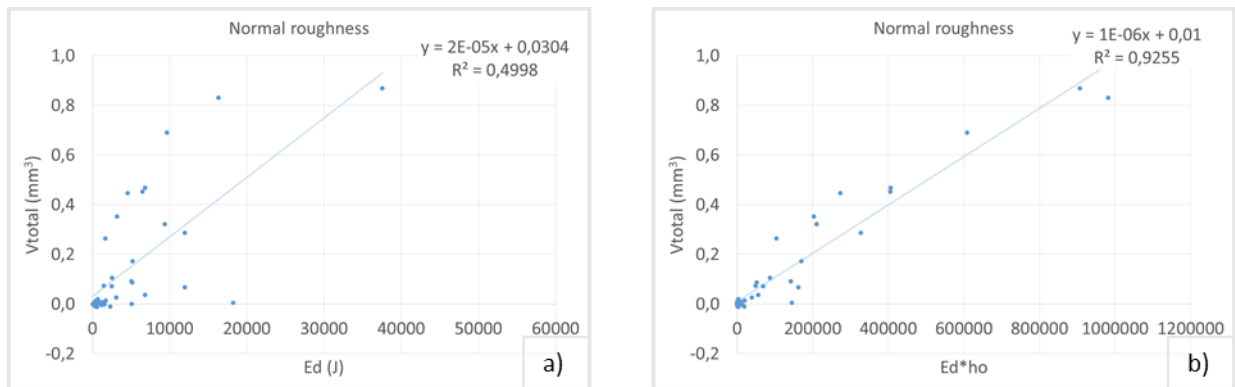
Figure 3.47. Linear regression of the evolution of the wear volume with a) The dissipated energy and b) The product of the dissipated energy by the displacement. For tests with normal roughness.
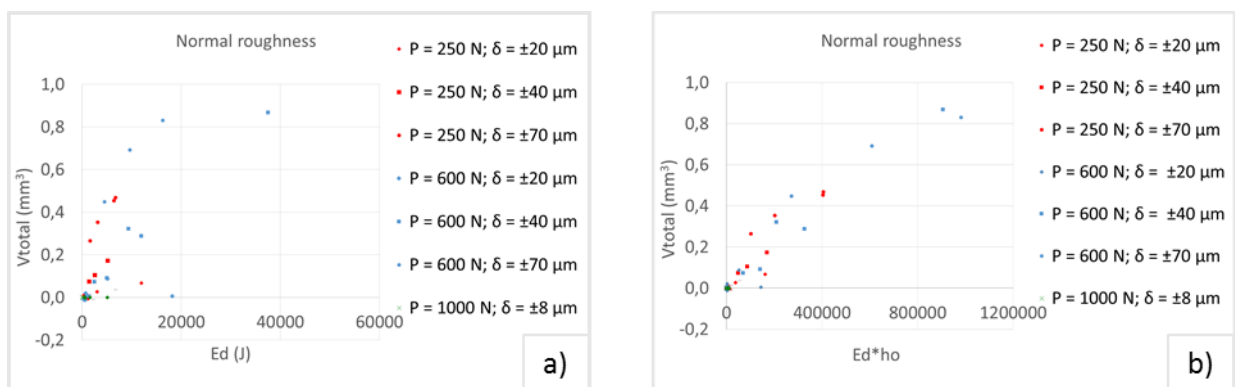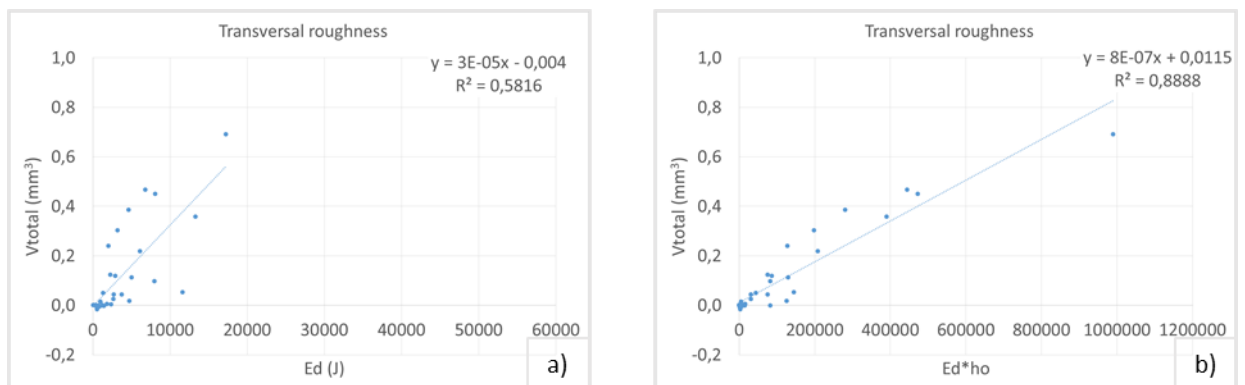

Figure 3.48. Linear regression of the evolution of the wear volume with a) The dissipated energy and b) The product of the dissipated energy by the displacement. For tests with transversal roughness.

This conclusion is consistent with what is stated in the bibliography [31].

It is also possible to conclude that the roughness direction has no significant importance for the wear volume.

3.5. Cracks analysis

The analysis of the cracks can give information about the conditions that the cracking threshold of the material is exceeded. Using the procedure described in section 2.4 and taking into account the tests that are willing to have cracks (in partial and mixed slip regime), an analysis of the length of the cracks that have been identified was done. Note that all tests in partial and mixed slip regime were evaluated.

For a displacement of ±20 μm and normal force of 250 N it was not observed significant cracks (because of wear). It was also found out that cracks only occurred for low displacement amplitude and high normal force, so that, only tests in these conditions were considered for the analysis of cracks.

Figure 3.49, Figure 3.50 and Figure 3.51 show the relation between the length of the cracks with the tangential force for the different displacement amplitude, for each number of cycles and normal force.
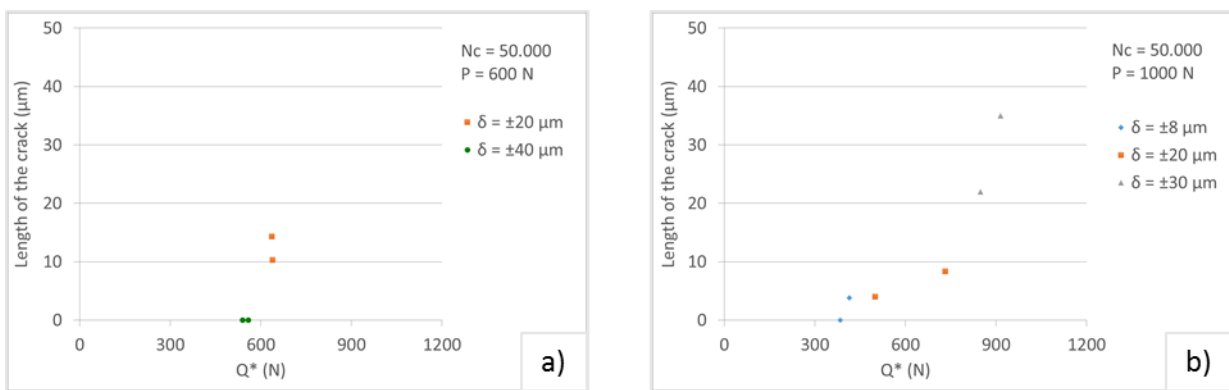
Figure 3.49. Evolution of the length of the crack with the tangential force for 50.000 cycles and with a normal force of a) 600 N and b) 1000 N.
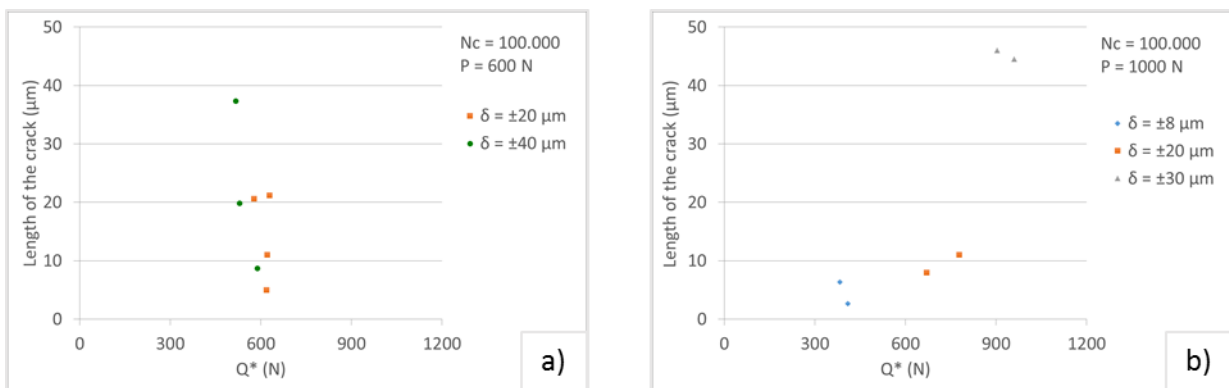
Figure 3.50. Evolution of the length of the crack with the tangential force for 100.000 cycles and with a normal force of a) 600 N and b) 1000 N.
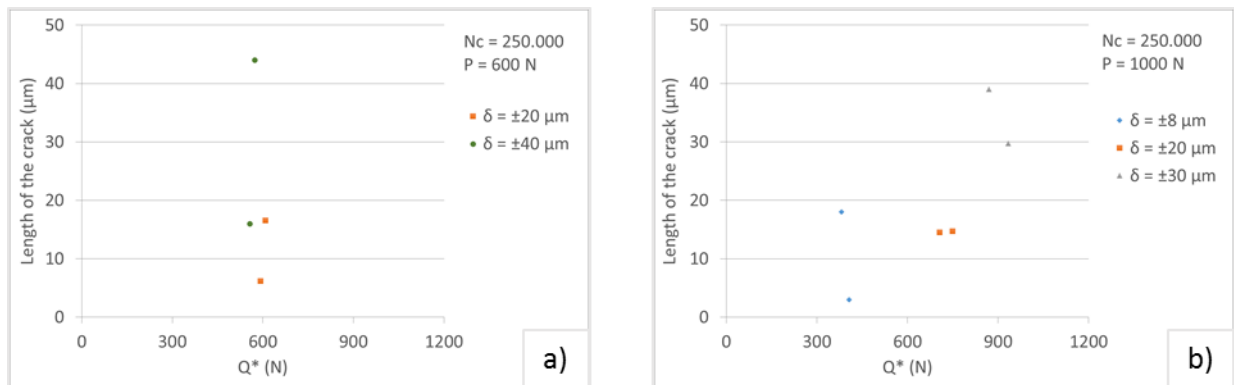
Figure 3.51. Evolution of the length of the crack with the tangential force for 250.000 cycles and with a normal force of a) 600 N and b) 1000 N.

When looking at the results, it can be seen that, for a displacement amplitude of ±8 μm and a normal force of 1000 N, the material withstands the solicitations to which it is subject, so the stresses were not enough to cause relevant cracks. Besides that, for tests with 1000 N, the maximum length of the crack was observed for 30μm of displacement amplitude for the 3 different number of cycles.

The Figure 3.52 presents the evolution of the length of the crack with the tangential force for the two different types of roughness for each normal force and displacement amplitude.
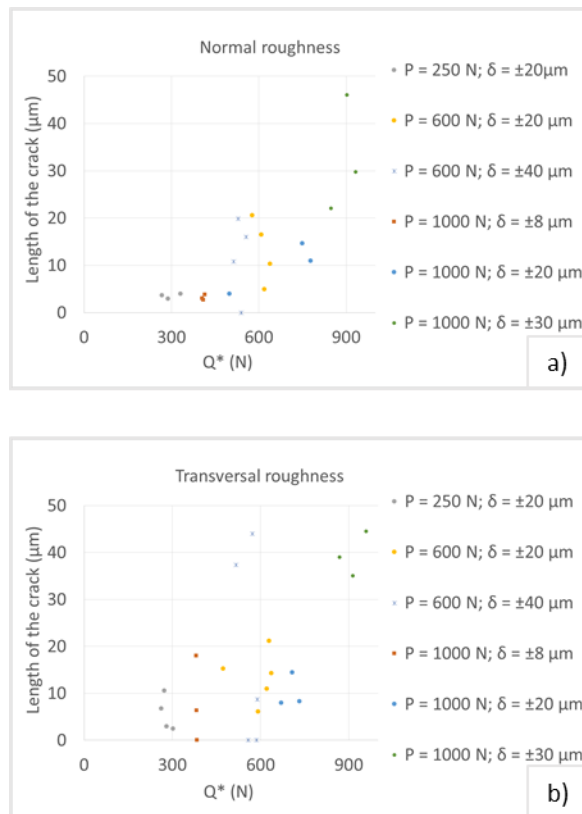
Figure 3.52. Evolution of the length of the crack with the tangential force for tests with a) Normal roughness and b) Transversal roughness.

As it is possible to see, the crack with a higher length was observed for a normal force of 1000 N, a displacement amplitude of ±30 μm and normal roughness although for transversal roughness also show higher values than the remaining tests. The discrepancy between the two roughness is not significant.

CONCLUSIONS

4. CONCLUSIONS

The ongoing concern in having a long and better life requires, inevitably, technological advances in health since this is the main factor at the top of the society daily concerns. Then, it becomes essential to improve the performance and create long lasting prosthesis that offers the patient a better quality of life.

As the fretting is one of the causes of failure of hip prostheses, the main objective of this thesis was to evaluate the fretting behaviour at the interface between the stem and neck adapter of a modular hip prosthesis, analysing the factors that contribute to this phenomenon.

Thus, the characterization performed in this study allowed the following conclusions:

1. It is observed that the friction coefficient is high (between 0,6 and 1,4).

2. Surface roughness has no big impact in friction coefficient in these conditions.

3. Wear volume is not very different for transversal roughness and for normal roughness.

4. It was confirmed that for higher displacement amplitude there will be more wear [23] [24].

5. For tests in gross slip regime, higher normal pressure will lead to higher wear rate, which consolidates the information in bibliography [26].

6. The amount of weight loss is higher for the highest number of load cycles [21].

7. It was observed the occurrence of adhesion phenomenon and transfer of material.

8. There is not a single relationship between dissipated energy and wear volume.

9. The formulation presented in the article [31] is proven in this study. Thus it is possible to confirm that, for titanium alloy, wear volume can be

Joana Filipa Jesus Pereira   63

normalized in a linear master curve, which allows to acknowledge the predisposition to adhesion of titanium alloy and to recognize the importance of the displacement amplitude on the wear volume, for this specific case.

10. Cracks occurred for low displacement amplitude and high normal force.

11. For a displacement amplitude of ±8 μm and a normal force of 1000 N (632 MPa) the stresses are not significant to cause relevant cracks.

12. For a displacement amplitude of ±20 μm and a normal force of 250 N (316 MPa) it was not observed significant cracks mainly due to the wear phenomenon.

13. The maximum length of a crack is observed for a displacement amplitude of ±30 μm and a normal force of 1000 N (632 MPa).

14. The direction of roughness has no influence in the length of the crack.

The study conducted was made in dry conditions and under more severe environment than in reality (*in vivo*), which makes it overestimated.

Since an *in vivo* implant is subjected to relative motion that causes the release of small debris that, in contact with body fluids, unleashes fretting corrosion, an approach about this subject should be done in order to assess the behaviour of the material under these conditions. Moreover, with cobalt-chromium being a viable alternative to titanium alloy, it also should be studied so that both materials can be compared.

BIBLIOGRAPHY

[1] T. Andrew Israel, Md, American Academy of Orthopaedic Surgeons, "Total Hip Replacement". Accessed in 28 of August 2015 in: http://orthoinfo.aaos.org/topic.cfm?topic=A00377&webid=24DAE050.

[2] J.A. Esperança Pina, 3ª Edição, "Anatomia humana da locomoção", LIDEL.

[3] OLGAKABEL, "Why do we get hip pain and what can we do about it?". Accessed in 12 of February 2015 in: http://sequencewiz.org/2014/04/23/get-hip-pain-can/.

[4] The Schmidt firm, PLLC, "What is a modular-neck hip implant?". Accessed in the 22 of August 2015 in: https://www.schmidtlaw.com/what-is-a-modular-neck-hip-implant/.

[5] Service d'Orthopédie Traumatologie, Hôpital Nord, CHU Amiens, Place Victor Pauchet (2013), "Les prothèses fémorales à col modulaire : Historique, évolution et expérience Amiénoise".

[6] Geoffrey Wright, MD, 1 Scott Sporer, MD, MS,1 Robert Urban, PhD,1 and Joshua Jacobs, MD1 (2010), "Fracture of a Modular Femoral Neck After Total Hip Arthroplasty", A Case Report, The journal of bone and and joint surgery.

[7] DePuy Hip Implants Worldwide Recall, "Defective Hip Implants". Accessed in 10 of February 2015 in: http://www.medrecallnews.com/home/hip-implants.

[8] P. Wodecki, D. Sabbah, G. Kermarrec, I. Semaan (2013), "New type of hip arthroplasty failure related to modular femoral components: Breakage at the neck-stem junction", Case Report, Orthopaedics & Traumatology: Surgery & Research, 741-744.

[9] M.B. Ellman, MD, B.R. Levine, MD, (2013), "Fracture of the Modular Femoral Neck Component in Total Hip Arthroplasty", Case Report, The Journal of Arthroplasty, Vol. 28 No. 1.

[10] T.M. Grupp, T. Weik, W. Bloemer, H.P. Knaebel, (2010), "Modular titanium alloy neck adapter failures in hip replacement - failure mode analysis and influence of implant material", BMC Musculoskeletal Disorders, 11:3.

[11] Monteiro J.M., Faculdade de Medicina da Universidade de Lisboa, "Classes de biomateriais" (PowerPoint presentation).

[12] J.-A. Epinette, MAÎTRISE ORTHOPÉDIQUE, "Cols modulaires de tiges fémorales en chrome-cobalt: une idée sérieuse qui pose de sérieux problémes?". Acessed in 4 of May 2015 in: http://www.maitrise-orthopedique.com/articles/cols-modulaire-de-tiges-femorales-en-chrome-cobalt-une-idee-serieuse-qui-pose-de-serieux-problemes-12.

[13] S.Y. Jauch, G. Huber, H. Haschke, K. Sellenschloh, M.M. Morlock (2014), "Design parameters and the material coupling are decisive for the micromotion at the

stem-neck interface of bi-modular hip implants", Medical Engineering & Physics 36, 300-307,

[14] Prof Ian D Learmonth, FRCScorrespondenceemail, Claire Young, FRCS, Prof Cecil Rorabeck, FRCS (2007), "The operation of the century: total hip replacement".

[15] J. Ding, S.B. Leen, I.R. McColl (2004), "The effect of slip regime on fretting wear-induced stress evolution", International Journal of Fatigue 26, 521-531.

[16] Yongqing Fu, Jun Wei, Andrew W. (2000), "Some considerations on the mitigation of fretting damage by the application of surface-modification technologies", Journal of Materials Processing Technology 99, 231-245.

[17] D. W. Hoeppner, V. Chandrasekaran, C. B. Elliott, Fretting Fatigue: "Current Technology and Practices", Edição 1367, ASTM International.

[18] V. Chaudhry, Satish V. Kailas (2013), "Damage quantification under sliding and seizure condition using first-of-a-kind fretting machine", Wear 305, 140-154.

[19] FRIDRICI Vincent - "Fretting d'un alliage de titane revenu et lubrifié: Application au contact aube / disque", Lyon: 2002. PhD.

[20] K.J. Kubiak, T.G. Mathia, S. Fouvry, "Interface roughness effect on friction map under fretting contact conditions", Tribology International 43, 1500-1507.

[21] Heredia S, Fouvry S. (2010), "Introduction of a new sliding regime criterion to quantify partial, mixed and gross slip fretting regimes: correlation with wear and cracking processes", Wear, 269: 515–24.

[22] M. Baxmann, S.Y. Jauch,, C. Schilling, W. Blomer, T.M. Grupp, M.M. Morlock (2013), "The influence of contact conditions and micromotions on the fretting behavior of modular titanium alloy taper connections", Medical Engineering & Physics 35: 676-683.

[23] S. Fouvry, T. Liskiewicz, Ph. Kapsa, S. Hannel, E. Sauger (2003), "An energy description of wear mechanisms and its applications to oscillating sliding contacts", Wear 255: 287–298.

[24] S. Fouvry *, Ph. Kapsa, L. Vincent (1995), "Analysis of sliding behaviour for fretting loadings: determination of transition criteria", Wear 185: 35- 46.

[25] CETIM Interfaces (2014), Optimisation de la résistance au fretting des jonctions modulaires de prothèses de hanches" (PowerPoint presentation).

[26] K.J. Kubiak, T.W. Liskiewicz, T.G. Mathia (2011), "Surface morphology in engineering applications: Influence of roughness on sliding and wear in dry fretting", Tribology International 44: 1427-1432.

[27] M. Viceconti, M. Baleani, S. Squarzoni, A. Toni (1997), "Fretting wear in a modular neck hip prosthesis", Journal of Biomedical Materials Research, Vol. 35: 207-216.

[28] J. D. Bobyn, A. R. Dujovne, J. J. Krygier, and D. L. Young (1993), ''Surface analysis of the taper junctions of retrieved and in vitro tested modular hip prostheses,'' in Biological, Material, and Mechanical Considerations of Joint Replacement", B. F. Morrey (ed.), Raven Press, New York, pp. 287–301.

[29] Longqiu Li, Izhak Etsion, Frank E. Talke (2011), "The effect of frequency on fretting in a micro-spherical contact", Wear 270, 857-865.

[30] Laboratoire de Tribologie et Dynamique des Systèmes (2014), "Topographie de surface" (PowerPoint presentation).

[31] C. Paulin, S. Fouvry, S. Deyber (2005), "Wear kinetics of Ti-6Al-4V under constant and variable fretting sliding conditions", Wear 259: 292-299.

[32] SEM – Science et médicine, Fabricant François, TIGE XO À COL MODULAIRE. Accessed in 20 of March 2015 in: http://www.science-et-medecine.fr/hanche/tiges-femorales/a-cimenter/.

[33] Katsuhiko Maehara, Kenji Doi, Tomiharu Matsushita and Yoshio Sasaki (2002), "Application of Vanadium-Free Titanium Alloys to Artificial Hip Joints", Materials Transactions, Vol. 43, No. 12, pp 2936 to 2942. Special Issue on Biomaterials and Bioengineering.

[34] Standard Specification for Wrought Titanium-6Aluminum-4Vanadium ELI (Extra Low Interstitial) Alloy for Surgical Implant Applications (UNS R56401), Designation: F136 – 12a, ASTM International.

[35] Ti6Al4V Titanium Alloy, Arcam EBM system, Arcam AB, Krokslätts Fabriker 27A, SE 431 37 Mölndal, Sweden.

[36] RENISHAW, apply innovation, "Interferometry explained". Accessed in the 29 of August 2013 in: http://www.renishaw.com/en/interfelometry-explained--7854.

ANNEX A

The Skewness and Kurtosis factors of roughness are used to get an idea of the shape and the number of peaks and valleys. Both factors are dimensionless.

S_{sk} (**Skewness**): profile asymmetry factor that allows checking the wear resistance of the surface.

S_{ku}(**Kurtosis**): Profile flattening factor that describes the probability density sharpness of the profile.

In the Figure NA.1 is possible to see the different situations for both factors and its interpretation.
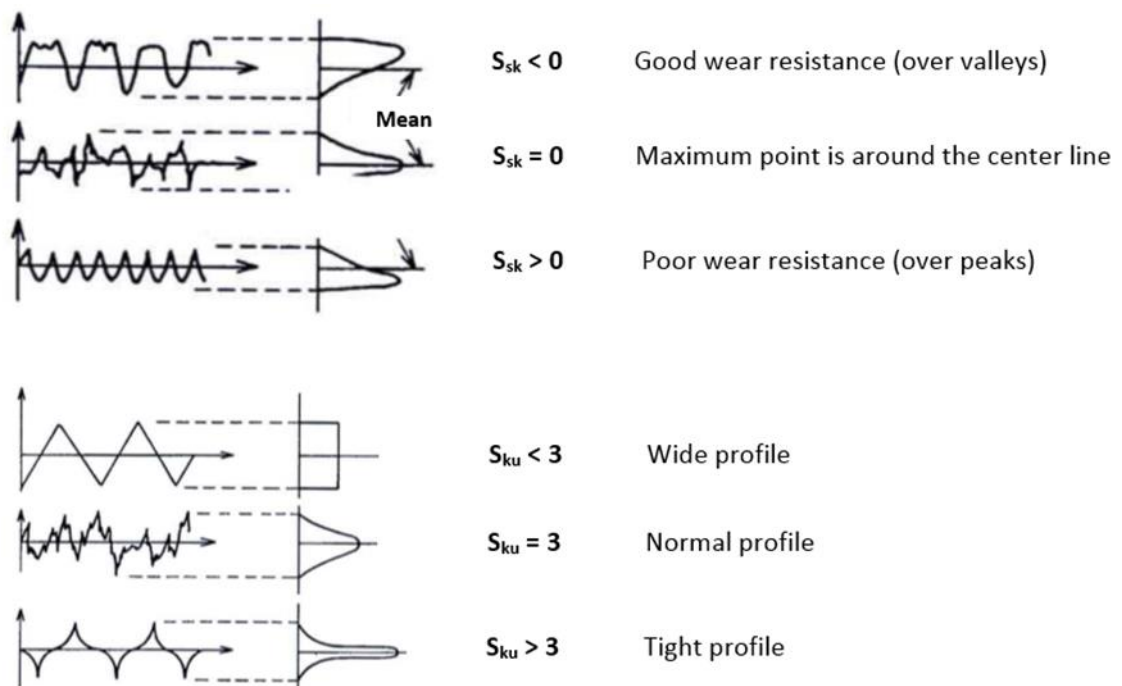

Figure NA.1. Interpretation on the Skewness and Kurtosis values.

ANNEX B

The equipment used to perform the test was the fretting set-up based on a MTS tension-compression hydraulic machine shown in Figure NB.1 and a MTS extensometer, placed (Figure NB.2) next to the contact in order to reach the various fretting regimes (gross, partial or mixed slip regime) and to limit the influence of the apparatus compliance.
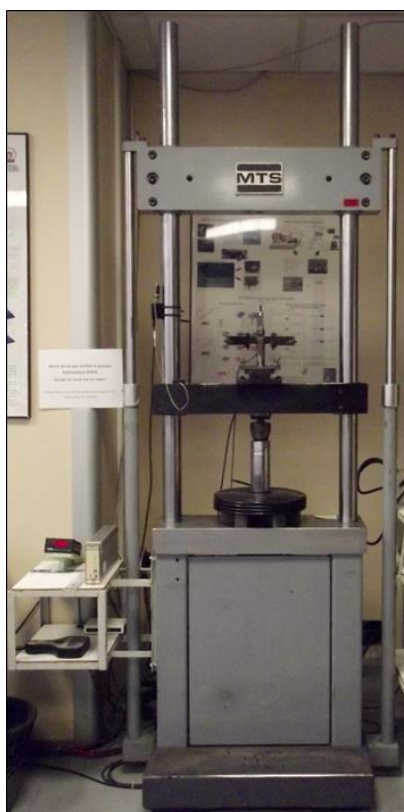

Figure NB.1. MTS tension-compression hydraulic machine.

Figure NB.2. MTS extensometer.

APPENDIX A

Considering equations (1.4), (1.5) and (1.6) for Hertz's theory, for a cylinder-on-flat configuration, the formulation for the contact pressure is the following:

$$P = \frac{p_0{}^2 \pi R L}{E^*} \tag{A.1}$$

For this study:

$E_1 = E_2 = 110$ Gpa

$\nu_1 = \nu_2 = 0{,}35$

$R = 10$ mm $= 0{,}01$ m

$L = 5$ mm $= 0{,}005$ m

So:

$$\frac{1}{E^*} = \left[\frac{1 - 0{,}35^2}{110}\right] + \left[\frac{1 - 0{,}35^2}{110}\right] \Leftrightarrow E^* \cong 62{,}68 \, GPa \tag{A.2}$$

In order to inquire about the values for cracks initiation, and considering the literature studied [13] [22], were admitted three values for contact pressure, 300, 500 and 800 MPa.

For these values, it was calculated the respective values for the normal force, as shown below.

For $p_0 = 300$ Mpa:

$$P = \frac{(300 \times 10^6)^2 \times \pi \times 0{,}01 \times 0{,}005}{62{,}68 \times 10^9} = 225{,}55 \, N \tag{A.3}$$

For $p_0 = 500$ Mpa:

$$P = \frac{(500 \times 10^6)^2 \times \pi \times 0,01 \times 0,005}{62,68 \times 10^9} = 626,51 \ N \tag{A.4}$$

For $p_0 = 800$ Mpa:

$$P = \frac{(800 \times 10^6)^2 \times \pi \times 0,01 \times 0,005}{62,68 \times 10^9} = 1603,88 \ N \tag{A.5}$$

Once the value imposed in the MTS machine is the normal force, and since it is done manually it is convenient to round the value.

Therefore the normal force assume the following values:

$P = 250$ N

$P = 600$ N

$P = 800$ N

Thus, it became necessary to use Hertz's theory again, but now to calculate the contact pressure for the new values of normal force.

For $P = 250$ N:

$$p_0 = \left(\frac{250 \times (62,68 \times 10^9)}{\pi \times 0,01 \times 0,005}\right)^{1/2} = 315845402,60 \ Pa = 315,85 \ MPa \tag{A.6}$$

For $P = 600$ N:

$$p_0 = \left(\frac{600 \times (62,68 \times 10^9)}{\pi \times 0,01 \times 0,005}\right)^{1/2} = 489305593,70 \ Pa = 489,31 \ MPa \tag{A.7}$$

For $P = 800$ N:

$$p_0 = \left(\frac{1000 \times (62,68 \times 10^9)}{\pi \times 0,01 \times 0,005}\right)^{1/2} = 631690805,20 \ Pa = 631,69 \ MPa \tag{A.8}$$

APPENDIX B

The contents from Figure PB.1 to Figure PB.9 shows the evolution of the wear volume with the dissipated energy for the different components, cylinder, flat and the total amount for each displacement amplitude, roughness and normal force.
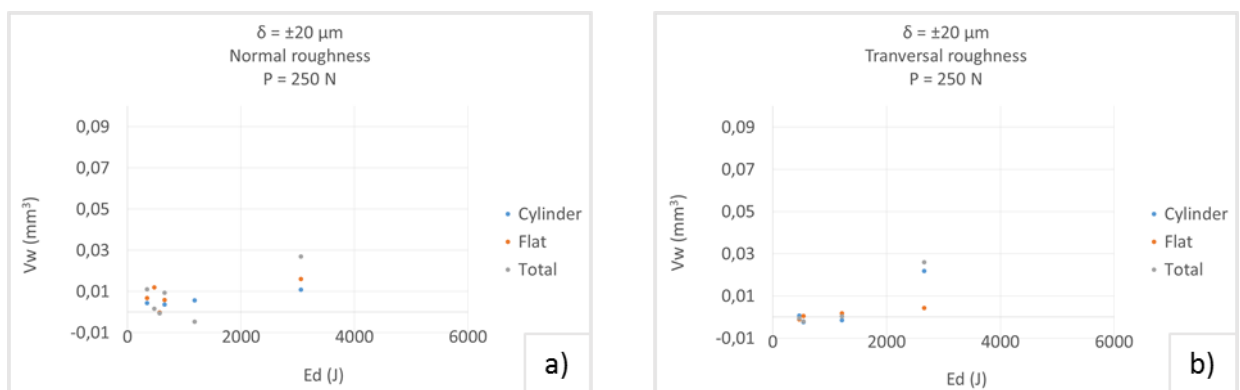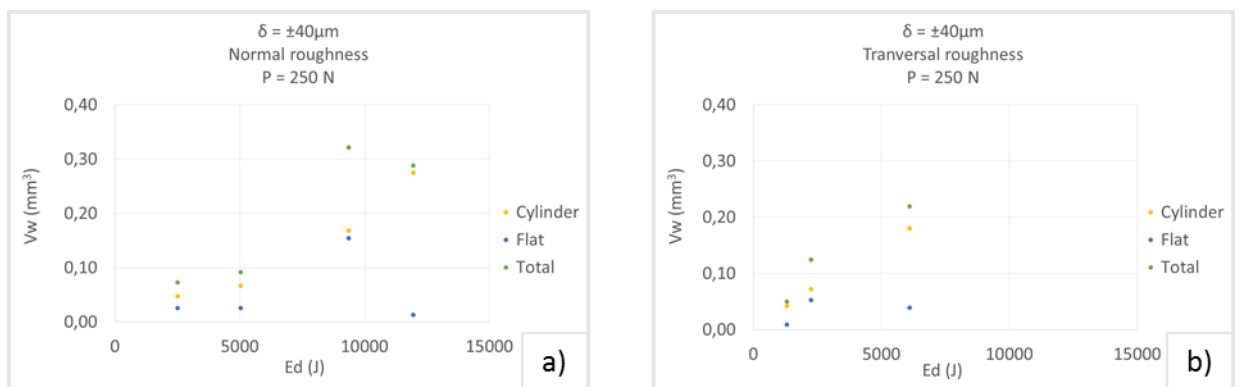

Figure PB.1. Evolution of wear volume with dissipated energy for the 2 components (cylinder and flat) and for the total amount (sum of both). For a displacement amplitude of ±20 μm, a normal force of 250N and a) Normal roughness and b) Transversal roughness.
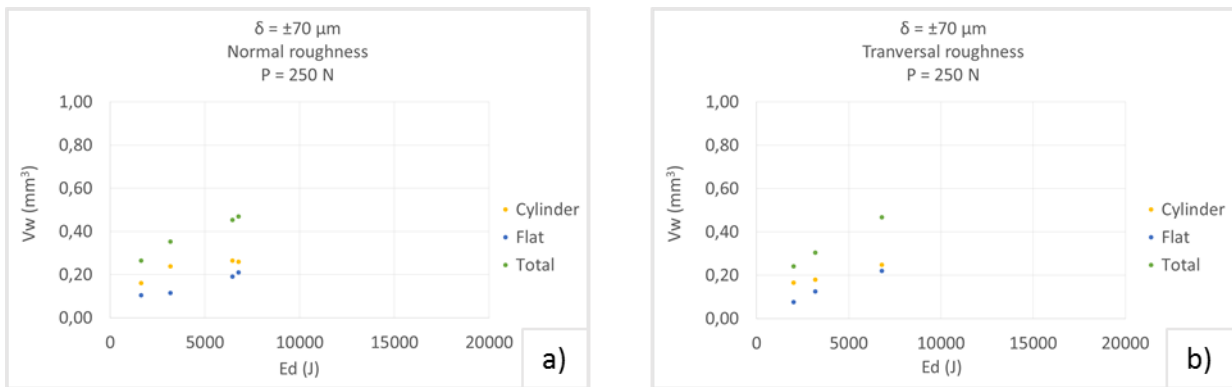

Figure PB.2. Evolution of wear volume with dissipated energy for the 2 components (cylinder and flat) and for the total amount (sum of both). For a displacement amplitude of ±40 μm, a normal force of 250N and a) Normal roughness and b) Transversal roughness.
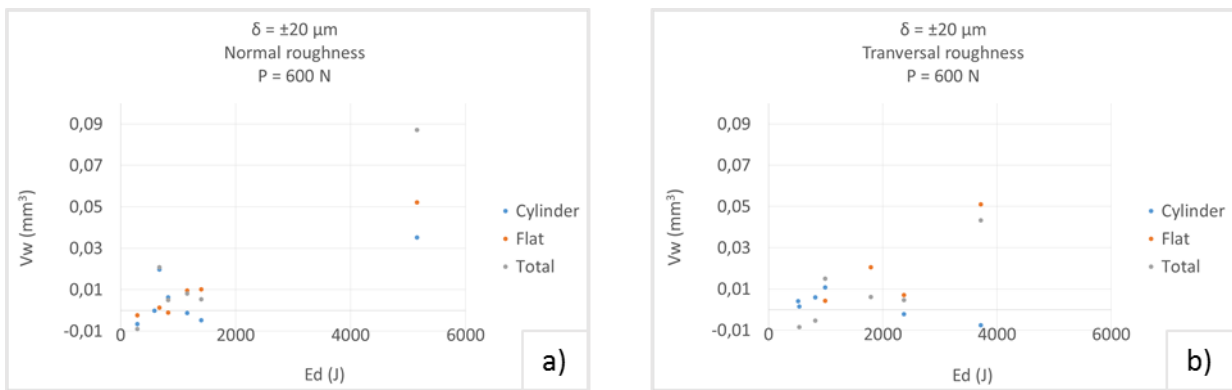
Figure PB.3. Evolution of wear volume with dissipated energy for the 2 components (cylinder and flat) and for the total amount (sum of both). For a displacement amplitude of ±70 µm, a normal force of 250N and a) Normal roughness and b) Transversal roughness.
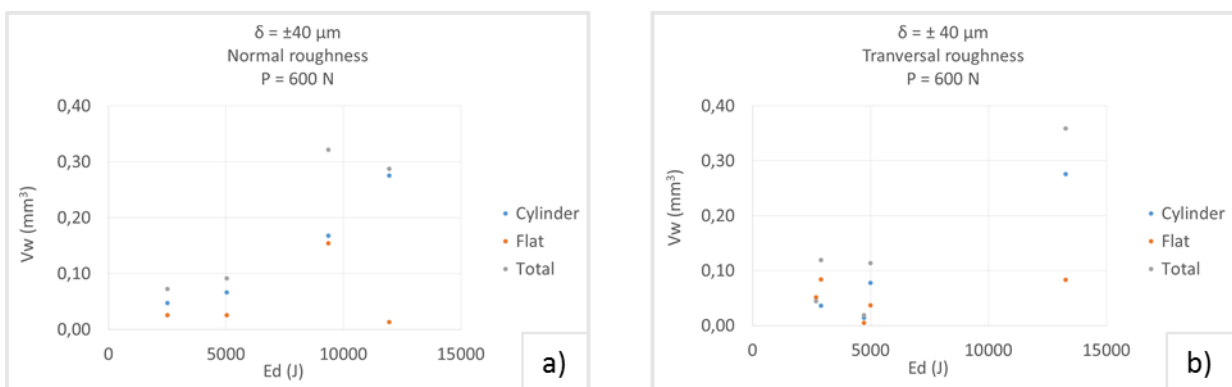

Figure PB.4. Evolution of wear volume with dissipated energy for the 2 components (cylinder and flat) and for the total amount (sum of both). For a displacement amplitude of ±20 µm, a normal force of 600N and a) Normal roughness and b) Transversal roughness.

Figure PB.5. Evolution of wear volume with dissipated energy for the 2 components (cylinder and flat) and for the total amount (sum of both). For a displacement amplitude of ±40 µm, a normal force of 600N and a) Normal roughness and b) Transversal roughness.
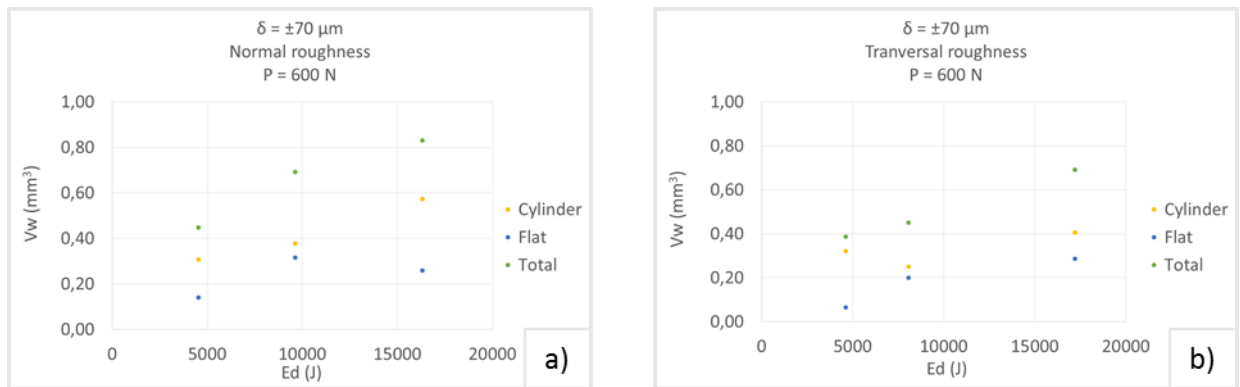
Figure PB.6. Evolution of wear volume with dissipated energy for the 2 components (cylinder and flat) and for the total amount (sum of both). For a displacement amplitude of ±70 μm, a normal force of 600N and a) Normal roughness and b) Transversal roughness.

Figure PB.7. Evolution of wear volume with dissipated energy for the 2 components (cylinder and flat) and for the total amount (sum of both). For a displacement amplitude of ±8 μm, a normal force of 1000N and a) Normal roughness and b) Transversal roughness.
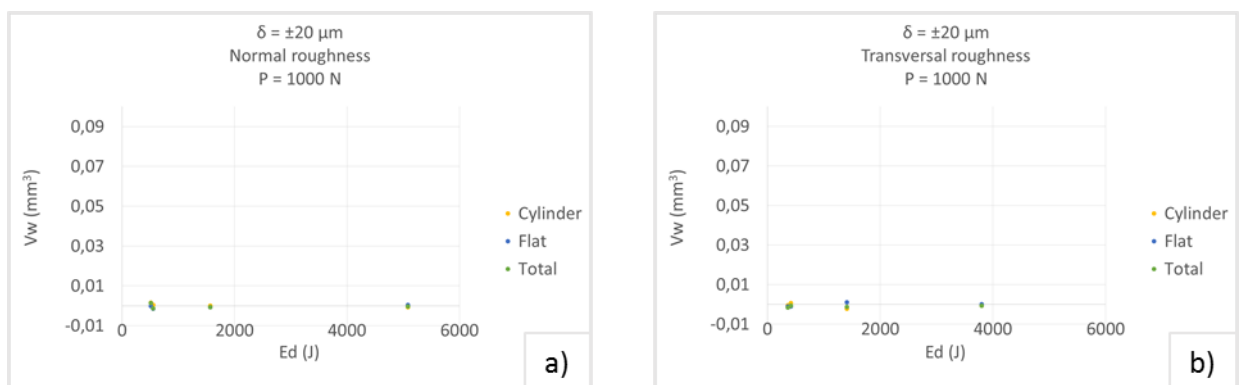

Figure PB.8. Evolution of wear volume with dissipated energy for the 2 components (cylinder and flat) and for the total amount (sum of both). For a displacement amplitude of ±20 μm, a normal force of 1000N and a) Normal roughness and b) Transversal roughness.
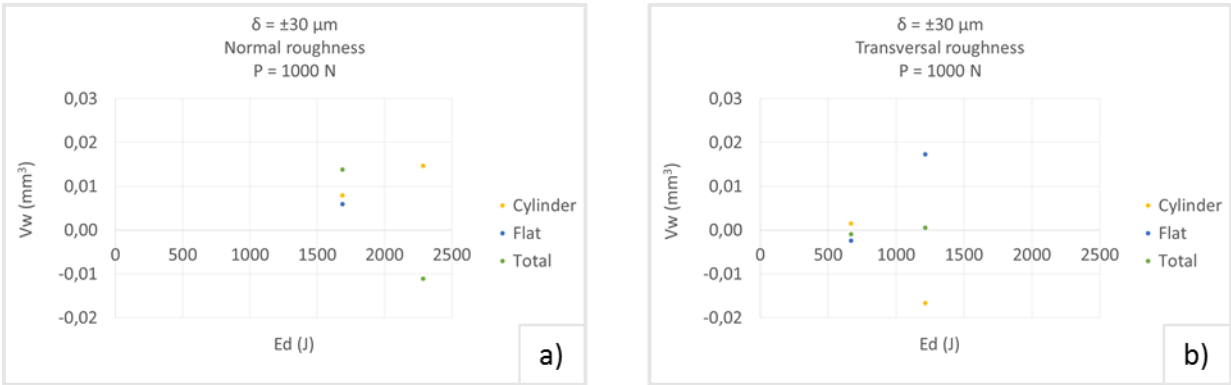
Figure PB.9. Evolution of wear volume with dissipated energy for the 2 components (cylinder and flat) and for the total amount (sum of both). For a displacement amplitude of ±30 μm, a normal force of 1000N and a) Normal roughness and b) Transversal roughness.